

Convergence History of the Songliao and Jiamusi Blocks in the Eastern End of Central Asian Orogenic Belt: Evidence from Detrital Zircons of Late Paleozoic Sedimentary Rocks



CHEN Zhaoxu¹, LIU Yongjiang^{2,3,*} and GUAN Qingbin²

¹ College of Earth Sciences, Jilin University, Changchun, Jilin 130061, China

² Key Lab of Submarine Geosciences and Prospecting Techniques, MOE, Institute for Advanced Ocean Study, College of Marine Geosciences, Ocean University of China, Qingdao, Shandong 266100, China

³ Laboratory for Marine Mineral Resources, Qingdao National Laboratory for Marine Science and Technology, Qingdao, Shandong 266237, China

Abstract: Central Asian Orogenic Belt (CAOB) is one of the largest accretionary orogenic belts in the world. The eastern segment of CAOB is dominated by Paleozoic Paleo Asian Ocean tectonic regime, Mesozoic Paleo-Pacific tectonic regime and Mongolian-Okhotsk tectonic regime. The Songliao and Jiamusi blocks are located in the easternmost part of the CAOB and are the key region to solve the problem about overprinting processes of multiple tectonic regimes. It is generally believed that the Mudanjiang Ocean between the two blocks was finally closed in the Mesozoic, but the Paleozoic magmatism also developed along the Mudanjiang suture zone, while on both sides of the suture zone, there were comparable Paleozoic strata, indicating that the two blocks had converged during the Paleozoic, and the evolution history of the two blocks in the Late Paleozoic remains controversial. The Carboniferous-Permian terrestrial strata mainly developed in Binxian, Wuchang and Tieli on Songliao Block, Baoqing and Mishan on Jiamusi Block. Samples from the Songliao and Jiamusi blocks in the Late Carboniferous-Early Permian and Late Permian are collected for comparative analysis. The LA-ICP-MS zircon U-Pb dating results show that the maximum depositional age of Middle Permian Tumenling Formation and Late Permian Hongshan Formation in Songliao Block is ~260 Ma, while that of Tatouhe Formation and Carboniferous strata in Jiamusi Block are ~290 Ma and ~300 Ma, respectively, which supports the previous stratigraphic division scheme. The age peaks of ~290–300 Ma, ~400 Ma, ~500 Ma appeared in the Late Carboniferous to Early Permian strata of Jiamusi Block and the Middle Permian strata of Songliao Block. The age peak of ~500 Ma in the Middle Permian strata of Songliao Block may come from the Cambrian basement, Mashan Complex, of Jiamusi Block, while the age peaks of ~420–440 Ma in the Carboniferous strata of Jiamusi Block may come from the Silurian magmatic arc in Zhangguangcai Range in the eastern margin of Songliao Block, reflects the history that they had been potential sources of each other, indicating that they may have combined in the Paleozoic. The Hongshan Formation of Songliao Block in the Late Permian lacks the age peak of ~500 Ma, which indicate that Jiamusi Block was not the provenance of Songliao Block in the Late Permian, that is, there was a palaeogeographic isolation between the two blocks. Combined with the ~210 Ma bimodal volcanic rocks developed along the Mudanjiang suture zone reported previously, we believe that the oceanic basin between the Songliao and Jiamusi blocks should have been connected in Late Permian and reopened during Late Permian to Late Triassic.

Key words: Detrital zircon, Permian stratum, Jiamusi Block, Songliao Block, Central Asian Orogenic Belt

Citation: Chen et al., 2019. Convergence History of the Songliao and Jiamusi Blocks in the Eastern End of Central Asian Orogenic Belt: Evidence from Detrital Zircons of Late Paleozoic Sedimentary Rocks. *Acta Geologica Sinica (English Edition)*, 93(5): 1417–1433. DOI: 10.1111/1755-6724.14392

1 Introduction

The eastern part of NE China lies in the junction of the easternmost segment of the Central Asian Orogenic Belt and the Pre-Pacific tectonic domain. It's long-term and complex orogeny from the Early Paleozoic to the Mesozoic has led to many controversies over the recovery of the tectonic evolution history, especially the Paleozoic (Sengör et al., 1993; Xiao et al., 2003; Li, 2006; Jian et al., 2008; Xu et al., 2015). The micro-continental blocks in the eastern segment of the CAOB are held between the Solonker-XarMoron-Changchun-Yanji suture zone in the

South and the Mongolia-Okhotsk suture zone in the north. From west to east, these are Erguna, Xing'an, Songliao and Jiamusi blocks (Zhang et al., 2006; Liu et al., 2010, 2017 and references therein). Erguna and Xing'an blocks were amalgamated in the early Cambrian (Li, 1991; Ge et al., 2005; Zhou et al., 2015; Feng et al., 2016); Xing'an and Songliao blocks were amalgamated at the end of early Carboniferous (Zhang et al., 2012; Liu et al., 2017). Apart from the controversial Jiamusi Block, the blocks in NE China may have amalgamated at the end of the Late Paleozoic and participated in the final closure of the Paleo Asian Ocean as a whole, i.e. the Jiamusi-Mongolian Block as previously proposed (Wang et al., 2008).

* Corresponding author. E-mail: liuyongjiang@ouc.edu.cn

The boundary between Songliao and Jiamusi blocks is the Heilongjiang complex along the Mudanjiang-Yilan suture zone. The Heilongjiang complex is divided into Proterozoic supracrustal rocks in the earlier geological survey and belongs to the basement unit together with the Mashan Complex (HBGMR, 1993). Because the blue schist in this unit is a significant sign of orogenesis, it has clockwise P-T-t paths (Bai et al., 1988; Zhang, 1992; Zhou et al., 2009; Zhao et al., 2010; Li et al., 2010, 2014), researchers gradually realized that Heilongjiang complex is a tectonic melange, which is the product of the combination of Songliao and Jiamusi blocks (Cao et al., 1992; Zhang, 1992; Ye et al., 1994). There are many viewpoints on the assemblage time reflected by the Heilongjiang Complex, including Proterozoic (Cao et al., 1992), Early Paleozoic (Xie et al., 2008) and Late Paleozoic (Li et al., 2009), but a lot of recent chronological evidence indicates that the final assemblage time of the two blocks should be Middle Jurassic to Early Cretaceous (Wu et al., 2007; Zhou et al., 2009; Li et al., 2009, 2011; Zhu et al., 2017a, b, c; Aouizerat et al., 2019). Early Paleozoic syn- and post-orogenic granitoids (Xu et al., 2012; Wang et al., 2012; Wang et al., 2016, 2017) along both sides of the Mudanjiang suture zone and Devonian strata (Meng et al., 2010; Li et al., 2019) with similar age composition of detrital zircons show the possibility that Songliao and Jiamusi blocks were once integrated during the Paleozoic.

The stability of zircon U-Th-Pb isotope system makes it able to reflect the nature of source area well after weathering, transportation and deposition. Provenance analysis of terrestrial basins is one of the important means to recover the evolution history of orogenic belts (Andersen, 2005; Gehrels, 2011). In the absence of igneous and metamorphic rocks records related to Paleozoic orogeny in the study area, provenance analysis becomes more important. At present, there are few studies on the provenance of the Late Paleozoic strata in the study area, especially the study on the Permian strata, as the crucial period of transformation between tectonic domains (Wilde et al., 2015), is lacking. In this work, LA-ICP-MS U-Pb dating of sandstone detrital zircons from Carboniferous and Permian terrestrial strata in both of Songliao and Jiamusi blocks, provenance analysis and comparison are carried out in order to recover the assembling history of the two blocks during the Late Paleozoic.

2 Geological Setting

The Songliao and Jiamusi blocks located in the eastern margin of the Central Asian Orogenic Belt. The Songliao Block is bounded by Heihe-Hegenshan suture zone with Xing'an Block to the west, while the eastern boundary is Mudanjiang-Yilan suture zone where Heilongjiang complex is exposed. The eastern margin of Songliao Block is composed of Mesozoic intrusions in Lesser Xing'an Range and Zhangguangcai Range. There is no large-scale Precambrian basement. Only a few ancient igneous rocks outcrops (Quan et al., 2013; Wang et al., 2014; Luan et al., 2017) in Lesser Xing'an Range and

Zhangguangcai Range show the possibility of the existence of the Precambrian basement. The Jiamusi Block is the easternmost microcontinent of the CAOB, bounded by the Yuejinshan fault to the east, which connected with Jurassic accreted Raohe complex (Wandashan Terrane) in the east (Fig. 1). The basement of Jiamusi Block is composed of old metamorphic basement, Mashan Complex, and Paleozoic igneous rocks (Wilde et al., 1997, 2000, 2003; Wu et al., 2001; Huang et al., 2009; Zhou et al., 2010 a, b; Yang et al., 2014, 2018; Chen et al., 2018; Hao et al., 2018; Han et al., 2019).

The Mudanjiang-Yilan suture zone, i.e. the area where Heilongjiang complex is exposed (from north to south: Luobei, Yilan and Mudanjiang), is the boundary between Songliao and Jiamusi blocks (Zhang et al., 1992, 2006; Ye et al., 1994). Late Paleozoic strata are distributed on both sides of the boundary. The Carboniferous terrestrial strata of Jiamusi Block is mainly distributed in Baoqing and Mishan area (Fig. 1). The sequence from bottom to top includes dacite tuff with interbedded sandstone of Early Carboniferous Beixing Formation, greywacke with interbedded tuffaceous slate of Late Carboniferous Guangqing Formation and tuffaceous sandstone of Late Carboniferous-Early Permian Zhenzishan Formation (Fig. 2). This sequence may reflect the gradual weakening trend of magmatic activity during Carboniferous (HBGMR, 1993). The Carboniferous strata of Songliao Block is only distributed in the Maanshan area of Yanshou County, of which age is from Late Devonian to Early Carboniferous called Fuxingtun Formation.

The Permian of Songliao Block is mainly distributed in Binxian, Wuchang, Bayan and Yichun (Fig. 1). From the bottom to the top, the sequence includes terrestrial sandy slate of Early Permian Yangmugang Formation, marine-terrestrial sandy slate of Middle Permian Tumenling Formation, intermediate-acid volcanic rocks of Middle Permian Wudaoling Formation and terrestrial sandstone of Late Permian Hongshan Formation (Fig. 2). From the perspective of marine fossils, the Middle Permian Tumenling Formation can correspond to the Zhesi Formation in the western Great Xing'an Range (Wang et al., 2009a). The Permian of Jiamusi Block corresponds weakly to the west. The terrestrial sandstone of Early Permian Tatouhe Formation deposited continuously above the Zhenzishan Formation while the terrestrial sandstone of Late Permian Chengshan Formation contacts with the Tatouhe Formation in parallel unconformity, lacking the Middle Permian strata (HBGMR, 1993).

3 Samples and analytical methods

3.1 Samples

In this study, the Carboniferous-Permian detrital sedimentary rock samples were collected on both sides of the tectonic belt in order to make a comparison (Fig. 1). The location of sandstone 8 samples are given in Table 1 and Fig. 2. On the side of Songliao Block, the Early Permian Yangmugang Formation in the Southern Shangzhi is composed of sandy slate whose protolith is feldspar quartz sandstone (Sample 18BD01); 2 samples were collected from the Middle Permian Tumenling

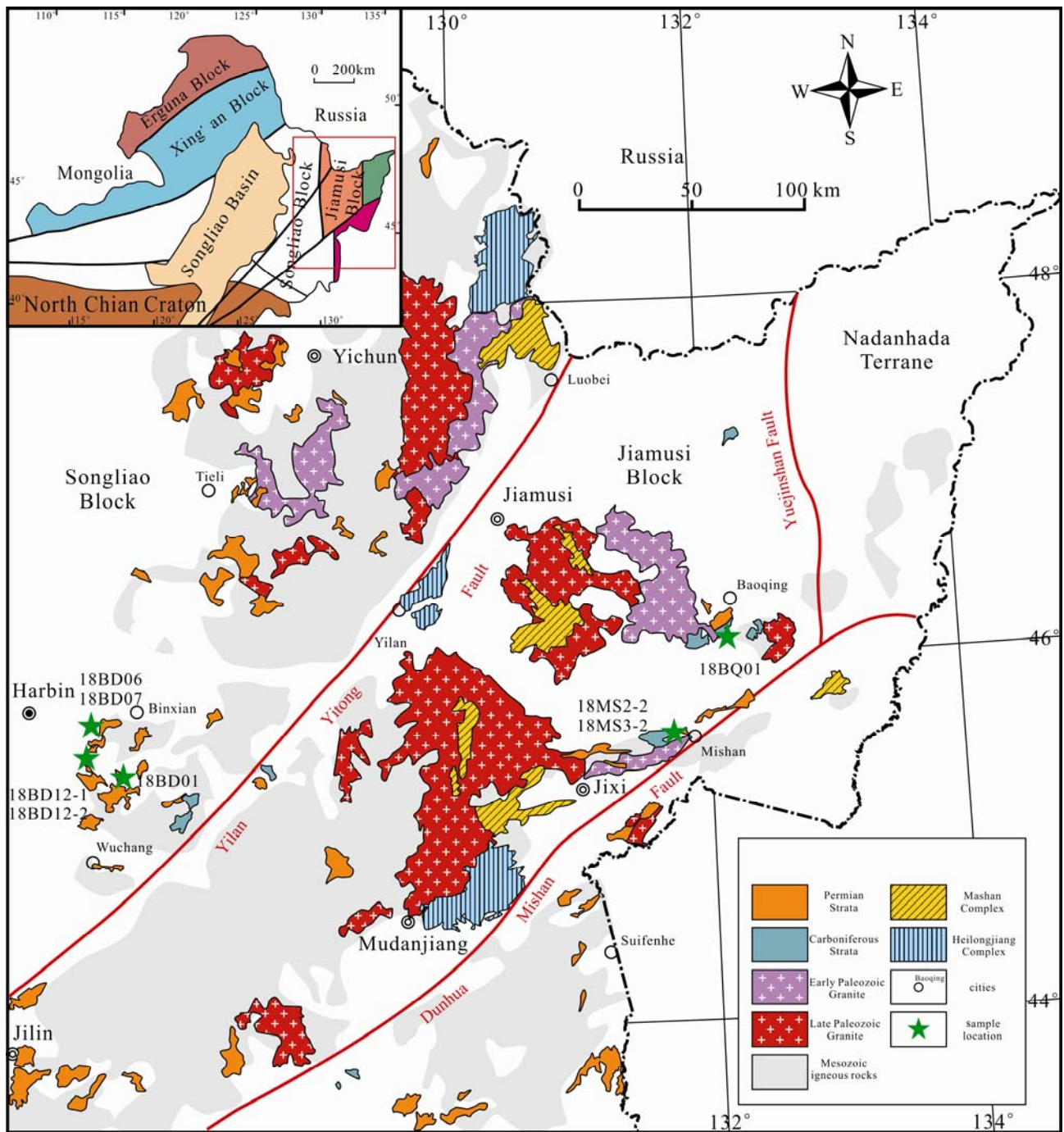


Fig. 1. Tectonic framework and late Paleozoic strata distribution map of the study area (after HBGMR, 1993; Wu et al., 2011; Liu et al., 2017).

Formation in the Eastern Acheng area which is composed of quartz sandstone with good abrasion (Sample 18BD06, 18BD07); Another two quartz sandstone samples with good sorting but poorly rounded were collected from the Late Permian Hongshan Formation in the Southeastern Acheng. These petrographic features suggest differences between Tumenling Formation and Hongshan Formation in sedimentary environments. On the other side, in Jiamusi Block, one sample from Early Permian Tatouhe Formation in the Southern Baoqing is quartz sandstone (18BQ01),

while 2 samples from Carboniferous strata (18MS2–2, 18MS3–2) are both feldspar quartz sandstone.

3.2 Analytical Methods

The zircon single mineral separation was completed by conventional methods: sorted by flotation and electromagnetic separation, and then selected manually under binoculars. Zircon LA-ICP-MS U-Pb dating was completed in the Key Laboratory of Mineral Resources Evaluation in Northeast Asia, Jilin University. ICP-MS is

Region		Songliao Block		Jiamusi Block	
		Formation	Lithology	Formation	Lithology
P	P ₃	Hongshan Fm. ★ 18BD12-1 ★ 18BD12-2	terrestrial sandstone	Chengshan Fm.	terrestrial sandstone
	P ₂	Wudaoling Fm.	intermediate-acid volcanic rocks	Hiatus	
	P ₁	Tumenling Fm. ★ 18BD06 ★ 18BD07	marine-terrestrial sandy slate		
		Yangmugang Fm. ★ 18BD01	terrestrial sandy slate	Tatouhe Fm. ★ 18BQ01	terrestrial sandstone
C	C ₂	Tangjiatun Fm.	rhyolite	Zhenzishan Fm. ★ 18MS2-2 ★ 18MS3-2	tuffaceous sandstone
	C ₁	Hiatus		Guangqing Fm.	greywacke with interbedded tuffaceous slate
				Beixing Fm.	dacite tuff with interbedded sandstone
				Qilikashan Fm.	dacitic tuff
D	Hiatus		Laotudingzi Fm.	rhyolite	
			Hiatus		
					Fuxingtun Fm.
	Heilonggong Fm.	marine sandstone with interbedded limestone	Heitai Fm.	glutenite with interbedded limestone	

Fig. 2. Late Paleozoic stratigraphic sequence in the Songliao and Jiamusi Blocks, showing the sample locations (after Wang et al., 2009a).

Table 1 Locations and lithology of 8 samples in this study

Geologic age	Sample No.	Location	GPS [x°x'x"]	Formation	Lithology
Middle Permian	18BD01	Southern Shangzhi	45°04'21.3"N 128°04'25.6"E	Yangmugang Fm.	feldspar quartz sandstone
Middle Permian	18BD06	Eastern Acheng	45°32'54.8"N 127°07'37.4"E	Tumenling Fm.	quartz sandstone
Middle Permian	18BD07	Eastern Acheng	45°33'04.9"N 127°09'05.6"E	Tumenling Fm.	quartz sandstone
Late Permian	18BD12-1	Southeastern Acheng	45°19'29.70" N 127° 9'3.80" E	Hongshan Fm.	quartz sandstone
Late Permian	18BD12-2	Southeastern Acheng	45°19'29.70" N 127° 9'3.80" E	Hongshan Fm.	quartz sandstone
Late Carboniferous	18MS2-2	Northern Mishan	45°31'29.31"N 131°48'19.26"E	Carboniferous strata	feldspar quartz sandstone
Late Carboniferous	18MS3-2	Northern Mishan	45°32'19.86"N 131°49'20.85"E	Carboniferous strata	feldspar quartz sandstone
Early Permian	18BQ01	Southern Baoqing	46°13'21.99"N 132° 5'35.67"E	Tatouhe Fm.	quartz sandstone

Agilent 7500a, the laser denudation system is GeoLas200M. The laser diameter is 32 μm , the frequency is 10 Hz, the gas background acquisition time of each analysis point is 20 s, and the signal acquisition time is 40 s. In order to avoid the widespread Pb-loss in ancient zircons (>1.0 Ga), $^{207}\text{Pb}/^{206}\text{Pb}$ age is used to represent the

reliable diagenetic age, and $^{206}\text{Pb}/^{238}\text{U}$ age is used for ages less than 1.0 Ga (Blank et al., 2003). Our data were plotted using Isoplot version 4.15 (Ludwig, 2012). Detrital zircon LA-ICP-MS U-Pb age analysis data are available in attached Table 2.

Table 2 U-Pb isotopic data for sandstone from 8 samples in this study (Only partially representative data are shown)

Analysis	Content (ppm)		Isotopic ratio						Corrected ages (Ma)						Concordance	
	Th	U	$\frac{^{238}\text{U}}{^{232}\text{Th}}$	$\frac{^{207}\text{Pb}}{^{206}\text{Pb}}$	1σ	$\frac{^{207}\text{Pb}}{^{235}\text{U}}$	1σ	$\frac{^{206}\text{Pb}}{^{238}\text{U}}$	1σ	$\frac{^{207}\text{Pb}}{^{206}\text{Pb}}$	1σ	$\frac{^{207}\text{Pb}}{^{235}\text{U}}$	1σ	$\frac{^{206}\text{Pb}}{^{238}\text{U}}$		1σ
18BD01																
20181230F04	230.06	487.31	2.118187	0.05377	0.00129	0.37009	0.00973	0.04991	0.00116	361	26	320	7	314	7	101.91
20181230F07	155.52	220.55	1.418146	0.05495	0.00158	0.46494	0.0141	0.06135	0.00145	410	31	388	10	384	9	101.04
20181230F11	164.8	267.23	1.621541	0.05571	0.00149	0.42889	0.01227	0.05584	0.0013	441	29	362	9	350	8	103.43
20181230F13	144.81	271.84	1.877218	0.05014	0.00143	0.2823	0.0085	0.04083	0.00096	201	32	252	7	258	6	97.67
20181230F14	510.62	830.63	1.626709	0.05271	0.00124	0.30225	0.0078	0.04159	0.00096	316	26	268	6	263	6	101.90
20181230F17	65.73	96.16	1.462955	0.05695	0.00184	0.61314	0.02058	0.0781	0.00187	490	36	486	13	485	11	100.21
20181230F27	268.36	687.99	2.563683	0.0577	0.00128	0.52219	0.01281	0.06565	0.00151	518	24	427	9	410	9	104.15
20181230F31	151.23	215.47	1.424783	0.05648	0.00139	0.57643	0.01532	0.07404	0.00171	471	26	462	10	460	10	100.43
20181230F32	93.05	229.53	2.466738	0.05389	0.0015	0.42994	0.01268	0.05787	0.00135	366	31	363	9	363	8	100.00
20181230F36	130.05	390.12	2.999769	0.05663	0.00131	0.59899	0.01521	0.07673	0.00177	477	25	477	10	477	11	100.00
20181230F39	355.37	695.4	1.956834	0.05248	0.00128	0.34089	0.00899	0.04713	0.00109	306	27	298	7	297	7	100.34
20181230F42	112.84	252.5	2.237682	0.05907	0.00144	0.6805	0.01794	0.08358	0.00193	570	26	527	11	517	11	101.93
20181230F43	126.02	310.26	2.46199	0.0556	0.00134	0.59337	0.01554	0.07743	0.00179	436	26	473	10	481	11	98.34
20181230F48	94.89	384.55	4.052587	0.05749	0.00133	0.63848	0.01618	0.08058	0.00185	510	25	501	10	500	11	100.20
20181230F70	218.15	197.02	0.90314	0.05687	0.00149	0.59774	0.01664	0.07628	0.00177	486	28	476	11	474	11	100.42
20181230F76	499.28	586.04	1.17377	0.05168	0.00129	0.29677	0.00793	0.04167	0.00096	271	27	264	6	263	6	100.38
20181230F77	102.62	160.96	1.568505	0.05453	0.00171	0.42611	0.01376	0.05671	0.00134	393	35	360	10	356	8	101.12
20181230F80	149.44	577.89	3.867037	0.0585	0.00152	0.67879	0.01872	0.08421	0.00195	549	27	526	11	521	12	100.96
18BD06																
20181230G07	271.57	378.34	1.393158	0.05131	0.00168	0.3017	0.01007	0.04274	0.001	255	38	268	8	270	6	99.26
20181230G20	184.29	547.46	2.970644	0.05584	0.00126	0.60364	0.01467	0.07856	0.00178	446	24	480	9	488	11	98.36
20181230G33	127.1	203.86	1.603934	0.05606	0.00136	0.64903	0.01684	0.0841	0.00192	455	26	508	10	521	11	97.50
20181230G48	243.36	472.23	1.940459	0.05385	0.00125	0.43479	0.01103	0.05862	0.00134	365	26	367	8	367	8	100.00
20181230G49	410.73	460.84	1.122002	0.05196	0.00122	0.38517	0.00987	0.05382	0.00123	284	26	331	7	338	8	97.93
20181230G50	32.33	88.63	2.741417	0.05707	0.0017	0.6525	0.02026	0.08299	0.00195	494	32	510	12	514	12	99.22
20181230G52	125.6	181.52	1.445223	0.05235	0.00151	0.33658	0.01022	0.04666	0.00109	301	32	295	8	294	7	100.34
20181230G54	247.72	1113.21	4.493824	0.05744	0.00126	0.55297	0.01343	0.06987	0.0016	508	24	447	9	435	10	102.76
20181230G58	146.57	148.88	1.01576	0.05322	0.00175	0.43312	0.01468	0.05904	0.00141	338	38	365	10	370	9	98.65
20181230G61	397.13	436.17	1.098305	0.05399	0.00144	0.38448	0.01096	0.05166	0.0012	371	29	330	8	325	7	101.54
20181230G62	353.39	676.55	1.914457	0.05668	0.00127	0.60681	0.01508	0.07766	0.00179	479	25	482	10	482	11	100.00
20181230G63	264.75	364.51	1.376808	0.05074	0.00154	0.30284	0.00963	0.04329	0.00102	229	35	269	8	273	6	98.53
20181230G64	234.94	370.15	1.575509	0.05262	0.00131	0.38488	0.01037	0.05305	0.00123	312	27	331	8	333	8	99.40
20181230G65	83.59	158.4	1.894964	0.05778	0.00163	0.60978	0.01827	0.07653	0.0018	521	30	483	12	475	11	101.68
20181230G67	141.86	247.35	1.74362	0.05065	0.00158	0.33404	0.01092	0.04782	0.00114	225	36	293	8	301	7	97.34
20181230G73	200.33	540.63	2.698697	0.05811	0.00134	0.55408	0.01418	0.06911	0.0016	390	118	423	16	429	10	98.60
20181230G77	167.31	314.79	1.881477	0.0566	0.00175	0.55248	0.01797	0.07072	0.00169	476	34	447	12	440	10	101.59
18BD07																
20181230H11	282.49	458.28	1.622288	0.05889	0.00134	0.70899	0.01799	0.08732	0.00203	563	25	544	11	540	12	100.74
20181230H13	429.5	1139.68	2.653504	0.0564	0.00122	0.50602	0.01235	0.06507	0.00151	468	24	416	8	406	9	102.46
20181230H19	182.83	319.14	1.745556	0.05261	0.00158	0.31058	0.00983	0.04282	0.00102	312	34	275	8	270	6	101.85
20181230H20	131.83	209.93	1.59243	0.0538	0.00162	0.31203	0.0099	0.04206	0.001	363	34	276	8	266	6	103.76
20181230H29	170.06	297.71	1.750617	0.05491	0.00165	0.4433	0.01405	0.05855	0.0014	409	33	373	10	367	9	101.63
20181230H35	133.54	115.26	0.863112	0.05433	0.00168	0.44141	0.01431	0.05893	0.00141	385	35	371	10	369	9	100.54
20181230H36	69.75	85.56	1.226667	0.05446	0.00188	0.44006	0.0157	0.0586	0.00142	390	40	370	11	367	9	100.82
20181230H37	48.38	201.64	4.167838	0.05235	0.00217	0.31175	0.01307	0.04319	0.00108	301	52	276	10	273	7	101.10
20181230H42	72.06	129.9	1.802664	0.05294	0.00275	0.34899	0.01809	0.04781	0.00126	326	71	304	14	301	8	101.00
20181230H51	154.9	205.71	1.328018	0.05885	0.00159	0.63749	0.01839	0.07857	0.00185	562	29	501	11	488	11	102.66
20181230H54	77.47	234.88	3.031883	0.05501	0.00141	0.62553	0.01735	0.08247	0.00193	413	28	493	11	511	11	96.48
20181230H61	143.46	252.34	1.758957	0.05841	0.00138	0.70753	0.01841	0.08786	0.00204	545	25	543	11	543	12	100.00
20181230H62	1148.19	918.27	0.799754	0.05736	0.00126	0.63015	0.01551	0.07968	0.00184	505	24	496	10	494	11	100.40
20181230H63	336.31	467.07	1.388808	0.05479	0.00129	0.44246	0.01149	0.05857	0.00136	404	26	372	8	367	8	101.36
20181230H64	407.23	1005.01	2.467917	0.05639	0.00125	0.50829	0.01255	0.06537	0.00151	468	24	417	8	408	9	102.21
20181230H70	212.5	668.8	3.147294	0.06098	0.00133	0.63892	0.01558	0.076	0.00175	461	107	468	15	469	11	99.79
20181230H76	116.15	289.76	2.494705	0.05568	0.00137	0.62529	0.0167	0.08145	0.00189	440	27	493	10	505	11	97.62
20181230H77	164.67	313.54	1.904051	0.0523	0.00158	0.31407	0.00993	0.04356	0.00103	299	34	277	8	275	6	100.73
18BD12-1																
20181229K04	203.26	213.04	1.048116	0.05747	0.00158	0.60229	0.01754	0.076	0.00179	510	29	479	11	472	11	101.48
20181229K12	192.46	420.89	2.186896	0.05664	0.00142	0.5976	0.01617	0.07653	0.00178	478	27	476	10	475	11	100.21
20181229K18	76.49	207.52	2.713034	0.05303	0.00176	0.3663	0.01255	0.0501	0.0012	330	38	317	9	315	7	100.63
20181229K29	58.14	93.77	1.612831	0.05469	0.00319	0.30552	0.01759	0.04052	0.00112	400	80	271	14	256	7	105.86
20181229K37	117.28	226.25	1.929144	0.05365	0.00156	0.34556	0.01063	0.04671	0.00111	356	32	301	8	294	7	102.38
20181229K38	20.09	18.93	0.94226													

Continued Table 2

Analysis	Content (ppm)		Isotopic ratio						Corrected ages (Ma)						Concordance	
	Th	U	$\frac{^{238}\text{U}}{^{232}\text{Th}}$	$\frac{^{207}\text{Pb}}{^{206}\text{Pb}}$	1σ	$\frac{^{207}\text{Pb}}{^{235}\text{U}}$	1σ	$\frac{^{206}\text{Pb}}{^{238}\text{U}}$	1σ	$\frac{^{207}\text{Pb}}{^{206}\text{Pb}}$	1σ	$\frac{^{207}\text{Pb}}{^{235}\text{U}}$	1σ	$\frac{^{206}\text{Pb}}{^{238}\text{U}}$		1σ
18BD12-2																
20181229L10	51.55	84.87	1.646363	0.05402	0.00211	0.34358	0.01362	0.04613	0.00113	372	47	300	10	291	7	103.09
20181229L19	159.17	127.7	0.802287	0.0528	0.00182	0.35552	0.01259	0.04883	0.00117	320	40	309	9	307	7	100.65
20181229L20	457.68	767.28	1.676455	0.05202	0.00127	0.32483	0.00861	0.04529	0.00104	286	27	286	7	286	6	100.00
20181229L24	61.41	52.24	0.850676	0.05246	0.00464	0.34485	0.02984	0.04767	0.00153	306	138	301	23	300	9	100.33
20181229L25	200.02	362.8	1.813819	0.05239	0.00142	0.34678	0.01002	0.04801	0.00112	302	30	302	8	302	7	100.00
20181229L36	64.28	65.29	1.015713	0.05326	0.00288	0.34287	0.01841	0.0467	0.00123	340	74	299	14	294	8	101.70
20181229L42	189.43	243.54	1.285646	0.05313	0.00151	0.36948	0.01108	0.05044	0.00118	334	31	319	8	317	7	100.63
20181229L43	39.51	61.26	1.550494	0.05532	0.00243	0.34631	0.01529	0.0454	0.00114	425	55	302	12	286	7	105.59
20181229L44	210.1	487.98	2.322608	0.05268	0.00129	0.32845	0.00873	0.04523	0.00104	315	27	288	7	285	6	101.05
20181229L45	121.23	155.33	1.281284	0.05301	0.00196	0.3489	0.0132	0.04774	0.00116	329	44	304	10	301	7	101.00
20181229L50	134.72	260.35	1.932527	0.05675	0.00141	0.57131	0.01536	0.07302	0.00169	482	27	459	10	454	10	101.10
20181229L51	29.2	49.74	1.703425	0.0526	0.0027	0.32989	0.01692	0.04549	0.00117	312	71	289	13	287	7	100.70
20181229L62	131.79	94.7	0.718567	0.05242	0.00186	0.3457	0.01259	0.04783	0.00115	304	42	301	9	301	7	100.00
20181229L63	1000.81	1693.46	1.692089	0.05383	0.00125	0.29941	0.00765	0.04034	0.00093	364	26	266	6	255	6	104.31
18BQ01																
20181229C04	1.36	3.31	2.433824	0.05643	0.00167	0.62891	0.01966	0.08083	0.00193	469	32	495	12	501	12	98.80
20181229C05	2.39	4.28	1.790795	0.05307	0.00169	0.3382	0.01127	0.04621	0.00111	332	36	296	9	291	7	101.72
20181229C08	1.82	3.38	1.857143	0.0527	0.0018	0.3331	0.0118	0.04584	0.00111	316	40	292	9	289	7	101.04
20181229C14	1.87	3.63	1.941176	0.05257	0.00176	0.33527	0.01165	0.04625	0.00111	310	39	294	9	291	7	101.03
20181229C16	4.63	12.36	2.669546	0.05629	0.00136	0.62401	0.01659	0.0804	0.00188	464	26	492	10	499	11	98.60
20181229C33	4.45	7.76	1.74382	0.05775	0.00176	0.66349	0.02124	0.08333	0.00199	520	33	517	13	516	12	100.19
20181229C35	3.53	7.45	2.110482	0.05701	0.0014	0.64316	0.01722	0.08182	0.00191	492	26	504	11	507	11	99.41
20181229C46	1.72	13.95	8.110465	0.06256	0.00165	0.68507	0.01936	0.07942	0.00187	436	99	479	14	488	11	98.16
20181229C65	6.27	12.74	2.031898	0.05872	0.00135	0.65791	0.01669	0.08127	0.00188	557	25	513	10	504	11	101.79
20181229C67	7.82	16.6	2.122762	0.05646	0.00144	0.51115	0.01407	0.06566	0.00153	471	27	419	9	410	9	102.20
20181229C68	5.53	6.52	1.179024	0.05347	0.00152	0.33696	0.01014	0.04571	0.00108	349	31	295	8	288	7	102.43
20181229C69	6.78	8.71	1.284661	0.05447	0.00144	0.33426	0.00948	0.04451	0.00104	391	29	293	7	281	6	104.27
20181229C70	3.77	12.29	3.259947	0.05714	0.00131	0.62964	0.01593	0.07992	0.00185	497	25	496	10	496	11	100.00
20181229C73	3.09	4.66	1.508091	0.05316	0.00169	0.33212	0.01098	0.04531	0.00108	336	36	291	8	286	7	101.75
20181229C74	4.27	17.24	4.037471	0.07046	0.00149	1.42608	0.03405	0.14679	0.00337	942	22	900	14	883	19	101.93
20181229C75	4.83	13.66	2.828157	0.05729	0.00129	0.63765	0.01588	0.08072	0.00186	503	24	501	10	500	11	100.20
20181229C76	18.86	40.77	2.161718	0.07166	0.0015	0.64409	0.01522	0.06519	0.0015	443	136	406	18	399	9	101.75
20181229C77	11.61	32.71	2.817399	0.08073	0.00167	1.29389	0.03029	0.11624	0.00267	821	105	727	22	696	16	104.45
20181229C92	5.61	6.59	1.174688	0.05263	0.00151	0.34423	0.01043	0.04743	0.00111	313	32	300	8	299	7	100.33
20181229C94	6.1	36.46	5.977049	0.05625	0.00124	0.50295	0.01231	0.06485	0.00149	462	24	414	8	405	9	102.22
20181229C103	12.08	12.6	1.043046	0.05254	0.0013	0.33563	0.00906	0.04633	0.00108	309	28	294	7	292	7	100.68
18MS2-2																
20181229A07	312.35	568.08	1.818729	0.05814	0.00135	0.64426	0.01681	0.08036	0.00188	535	25	505	10	498	11	101.41
20181229A17	247.35	895.07	3.618638	0.05633	0.00124	0.53689	0.01355	0.06913	0.00162	465	25	436	9	431	10	101.16
20181229A18	81.95	49.25	0.600976	0.1129	0.00269	5.1072	0.1366	0.32808	0.00779	1847	22	1837	23	1829	38	100.98
20181229A23	179.86	567.46	3.155009	0.05913	0.00135	0.64837	0.0168	0.07952	0.00187	572	25	507	10	493	11	102.84
20181229A24	92.93	139.55	1.501668	0.05392	0.00189	0.4351	0.016	0.05853	0.00141	368	42	367	11	367	9	100.00
20181229A36	63.63	165.08	2.594374	0.05416	0.00176	0.42903	0.01482	0.05745	0.00138	378	38	362	11	360	8	100.56
20181229A37	190.98	367.72	1.925437	0.05538	0.00142	0.43205	0.01223	0.05658	0.00134	428	28	365	9	355	8	102.82
20181229A38	159.93	384.04	2.401301	0.05462	0.0014	0.4348	0.01233	0.05773	0.00137	397	29	367	9	362	8	101.38
20181229A39	200.34	222.58	1.111011	0.05463	0.00157	0.43379	0.01348	0.05759	0.00137	397	33	366	10	361	8	101.39
20181229A42	129.64	208.2	1.605986	0.05961	0.00168	0.64875	0.01989	0.07893	0.00188	589	31	508	12	490	11	103.67
20181229A51	100.88	266.3	2.63977	0.05425	0.0015	0.41673	0.01258	0.05572	0.00133	381	31	354	9	350	8	101.14
20181229A52	70.76	105.76	1.49463	0.11217	0.00247	5.03643	0.12737	0.32565	0.00772	1835	21	1825	21	1817	38	100.99
20181229A54	221.75	138.46	0.624397	0.05452	0.00199	0.45129	0.01729	0.06003	0.00145	393	45	378	12	376	9	100.53
20181229A64	265.13	574.43	2.166598	0.05576	0.00155	0.54652	0.01657	0.07108	0.0017	443	31	443	11	443	10	100.00
20181229A65	490.32	527.51	1.075848	0.05538	0.00134	0.45428	0.01233	0.05949	0.00141	428	27	380	9	373	9	101.88
20181229A67	585.03	1815.34	3.102986	0.10868	0.00229	1.00893	0.02472	0.06733	0.00159	359	183	387	24	391	10	98.98
20181229A68	216.54	191.06	0.882331	0.05501	0.00229	0.45106	0.01943	0.05947	0.00147	413	54	378	14	372	9	101.61
20181229A69	191.4	489.38	2.556844	0.05798	0.00141	0.60527	0.01653	0.07572	0.0018	529	27	481	10	471	11	102.12
20181229A70	166.59	550.8	3.306321	0.05751	0.00131	0.62937	0.01636	0.07938	0.00188	511	25	496	10	492	11	100.81
20181229A71	233.48	392.52	1.681172	0.0558	0.00141	0.54032	0.01522	0.07023	0.00167	444	28	439	10	438	10	100.23
20181229A73	81.11	209.53	2.583282	0.05832	0.00195	0.43646	0.01543	0.05428	0.00131	403	140	348	16	339	8	102.65
20181229A74	60.49	238.52	3.943131	0.05611	0.00165	0.54274	0.01729	0.07016	0.00168	457	33	440	11	437	10	100.69
20181229A77	113.66	290.98	2.560092	0.05715	0.00141	0.62879	0.01736	0.07981	0.0019	497	27	495	11	495	11	100.00
18MS3-2																
20181229B04	62.57	175.61	2.806617	0.05466	0.00176	0.42999	0.01465	0.05706	0.0							

Continued Table 2

Analysis	Content (ppm)		Isotopic ratio					Corrected ages (Ma)					Concordance			
	Th	U	$\frac{^{238}\text{U}}{^{232}\text{Th}}$	$\frac{^{207}\text{Pb}}{^{206}\text{Pb}}$	1σ	$\frac{^{207}\text{Pb}}{^{235}\text{U}}$	1σ	$\frac{^{206}\text{Pb}}{^{238}\text{U}}$	1σ	$\frac{^{207}\text{Pb}}{^{206}\text{Pb}}$	1σ	$\frac{^{207}\text{Pb}}{^{235}\text{U}}$		1σ	$\frac{^{206}\text{Pb}}{^{238}\text{U}}$	1σ
20181229B31	167.43	319.67	1.909276	0.11289	0.00238	5.07943	0.12277	0.32632	0.00756	1846	20	1833	21	1821	37	101.37
20181229B32	379.12	952.43	2.512212	0.05628	0.00126	0.53099	0.01339	0.06843	0.00159	463	25	432	9	427	10	101.17
20181229B39	161.59	445.74	2.758463	0.05753	0.00139	0.58363	0.01563	0.07358	0.00171	512	26	467	10	458	10	101.97
20181229B42	86.16	199.29	2.313022	0.05712	0.00186	0.43388	0.01488	0.05509	0.0013	496	37	366	11	346	8	105.78
20181229B43	72.25	108.28	1.498685	0.05788	0.00193	0.55307	0.01938	0.0693	0.00164	525	39	447	13	432	10	103.47
20181229B46	78.53	135.51	1.725583	0.16382	0.00352	10.50791	0.25703	0.46521	0.01081	2495	18	2481	23	2463	48	101.30
20181229B55	56.43	376.72	6.675882	0.05739	0.0014	0.64307	0.01732	0.08126	0.00188	507	27	504	11	504	11	100.00
20181229B56	86.31	216.59	2.509443	0.05577	0.00165	0.53456	0.01687	0.06952	0.00163	443	33	435	11	433	10	100.46
20181229B69	633.08	1288.38	2.035098	0.05705	0.00149	1.05068	0.02527	0.10809	0.00249	725	116	672	23	656	15	102.44
20181229B70	295.33	901.66	3.053059	0.05743	0.00133	0.63884	0.01649	0.08067	0.00186	508	25	502	10	500	11	100.40
20181229B71	32.84	54.18	1.649817	0.11607	0.00271	5.47278	0.14237	0.34196	0.00797	1897	21	1896	22	1896	38	100.05
20181229B73	72.62	261.05	3.59474	0.05753	0.00153	0.53251	0.0154	0.06713	0.00156	512	29	433	10	419	9	103.34
20181229B74	31.69	266.43	8.407384	0.11449	0.00242	5.27047	0.12691	0.33386	0.0077	1872	20	1864	21	1857	37	100.81
20181229B75	134.53	345.19	2.565896	0.05731	0.00141	0.63832	0.01731	0.08078	0.00187	503	27	501	11	501	11	100.00
20181229B76	120.86	173.27	1.433642	0.11404	0.00246	5.26698	0.12871	0.33494	0.00774	1865	20	1864	21	1862	37	100.16
20181229B77	170.18	208.28	1.223881	0.05559	0.00154	0.53615	0.01596	0.06995	0.00163	436	31	436	11	436	10	100.00

4 Results

4.1 Samples in Songliao Block

Early Permian Yangmugang Formation (sample 18BD01; Fig. 3a; Fig. 4a): 80 zircon grains were chosen for U-Pb isotopic dating and 72 of them yielded concordant age results. The Th/U ratios range from 0.11 to 1.17 and most values of more than 0.4, indicating the magmatic origin (Wu and Zheng, 2004). The weighted mean $^{206}\text{Pb}/^{238}\text{U}$ ages of zircons <1.0 Ga range from 260 to 887 Ma, of which 6 peaks are 260–281 Ma (n=18), 290–318 Ma (n=9), 331–363 Ma (n=10), 384–428 Ma (n=10), 460–485 Ma (n=11) and 500–521 Ma (n=5). The age distribution range is very wide, and most of them are granular magmatic zircons with fine oscillatory zones. However, the youngest age peak of 260–281 Ma contains both granular and tabular zircons. Both granular and tabular zircons exist in the age peak of ~500–521 Ma, including two metamorphic zircon rim ages with ~500 Ma. The weighted mean $^{206}\text{Pb}/^{207}\text{Pb}$ ages of >1.0 Ga zircons consist of two grains, 1671±21 Ma and 2654±18 Ma, both of which are the core of the captured zircons.

Middle Permian Tumenling Formation (sample 18BD06; Fig. 3b; Fig. 4b): 60 zircon grains were chosen for U-Pb isotopic dating and 58 of them yielded concordant age results. The Th/U ratios range from 0.12 to 1.56. The weighted mean $^{206}\text{Pb}/^{238}\text{U}$ age of zircons <1.0 Ga range from 267 to 906 Ma. There are five Phanerozoic age peaks: 267–286 Ma (n=13), 294–317 Ma (n=9), 324–338 Ma (n=8), 429–440 Ma (n=7), 482–521 Ma (n=6). The weighted mean $^{206}\text{Pb}/^{207}\text{Pb}$ age of zircons >1.0 Ga is only one grain of 1293±21 Ma.

Middle Permian Tumenling Formation (sample 18BD07; Fig. 3c; Fig. 4c): 60 zircon grains were chosen for U-Pb isotopic dating and all of them yielded concordant age results. Th/U ratios range from 0.11 to 1.25, and most of them were >0.4. The weighted mean $^{206}\text{Pb}/^{238}\text{U}$ age of zircons <1.0 Ga is 266–946 Ma, with five Phanerozoic age peaks: 266–277 Ma (n=10), 295–314 Ma (n=6), 367–371 Ma (n=6), 400–415 Ma (n=6), 486–511 Ma (n=15). The weighted mean $^{206}\text{Pb}/^{207}\text{Pb}$ age of zircons >1.0 Ga is 1006–1795 Ma. Similar with the

sample 18BD01, the age peak of ~500 Ma has tabular zircons, while the other age peaks are granular zircons.

Late Permian Hongshan Formation (sample 18BD12–1; Fig. 3d; Fig. 4d): 60 zircon grains were chosen for U-Pb isotopic dating and 50 of them yielded concordant age results. The Th/U ratios range from 0.36 to 1.78, all of which are magmatic zircons. The weighted mean $^{206}\text{Pb}/^{238}\text{U}$ age of zircons <1.0 Ga is in the range of 250–475 Ma, with only one peak of 250–300 Ma, in which 286–287 Ma is highly concentrated (n=9). The weighted mean $^{206}\text{Pb}/^{207}\text{Pb}$ age of zircons >1.0 Ga is only one grain of 1832±20 Ma.

Late Permian Hongshan Formation (sample 18BD12–2; Fig. 3e; Fig. 4e): 60 zircon grains were chosen for U-Pb isotopic dating and 50 of them yielded concordant age results. The Th/U ratios range from 0.34 to 1.47. The weighted mean $^{206}\text{Pb}/^{238}\text{U}$ age of zircons <1.0 Ga is 255–454 Ma, with only one peak of 250–300 Ma. The age group of 288–293 Ma is highly concentrated (n=11), and the oldest age is 454±10 Ma.

4.2 Samples in Jiamusi Block

Carboniferous strata (sample 18MS2–2; Fig. 3g; Fig. 4g): 60 zircon grains were chosen for U-Pb isotopic dating and all of them yielded concordant age results. The Th/U ratios range from 0.14 to 1.66. The weighted mean $^{206}\text{Pb}/^{238}\text{U}$ age of zircons <1.0 Ga is in the range of 339–498 Ma, including three Phanerozoic age peaks: 359–364 Ma (n=14), 421–449 Ma (n=9), 471–498 Ma (n=11). The weighted mean $^{206}\text{Pb}/^{207}\text{Pb}$ age of zircons >1.0 Ga is 1783–1847 Ma.

Carboniferous strata (sample 18MS3–2; Fig. 3h; Fig. 4h): 60 zircon grains were chosen for U-Pb isotopic dating and all of them yielded concordant age results. The Th/U ratios range from 0.12 to 1.12. The weighted mean $^{206}\text{Pb}/^{238}\text{U}$ age of zircons <1.0 Ga is 302–803 Ma. There are three main Phanerozoic age peaks: 302–309 Ma (n=3), 416–436 Ma (n=23), 479–525 Ma (n=15). The weighted mean $^{206}\text{Pb}/^{207}\text{Pb}$ age of zircons >1.0 Ga is 1846–2495 Ma.

Early Permian Tatouhe Formation (sample 18BQ01; Fig. 3f; Fig. 4f): 80 zircon grains were chosen for U-Pb isotopic dating and 75 of them yielded concordant age

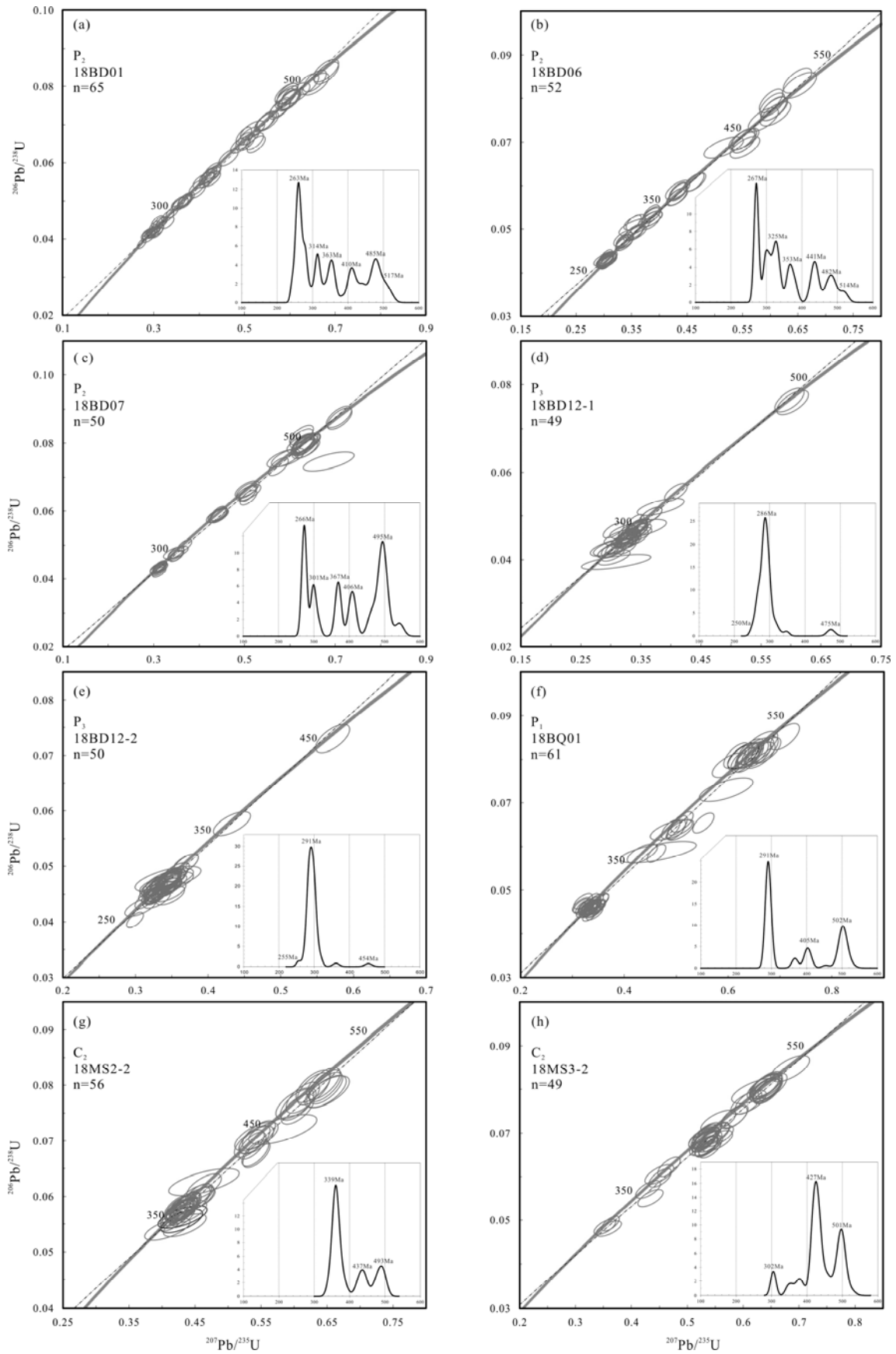


Fig. 3. U-Pb concordia diagram and age spectrum for detrital zircons of 8 samples in this study.

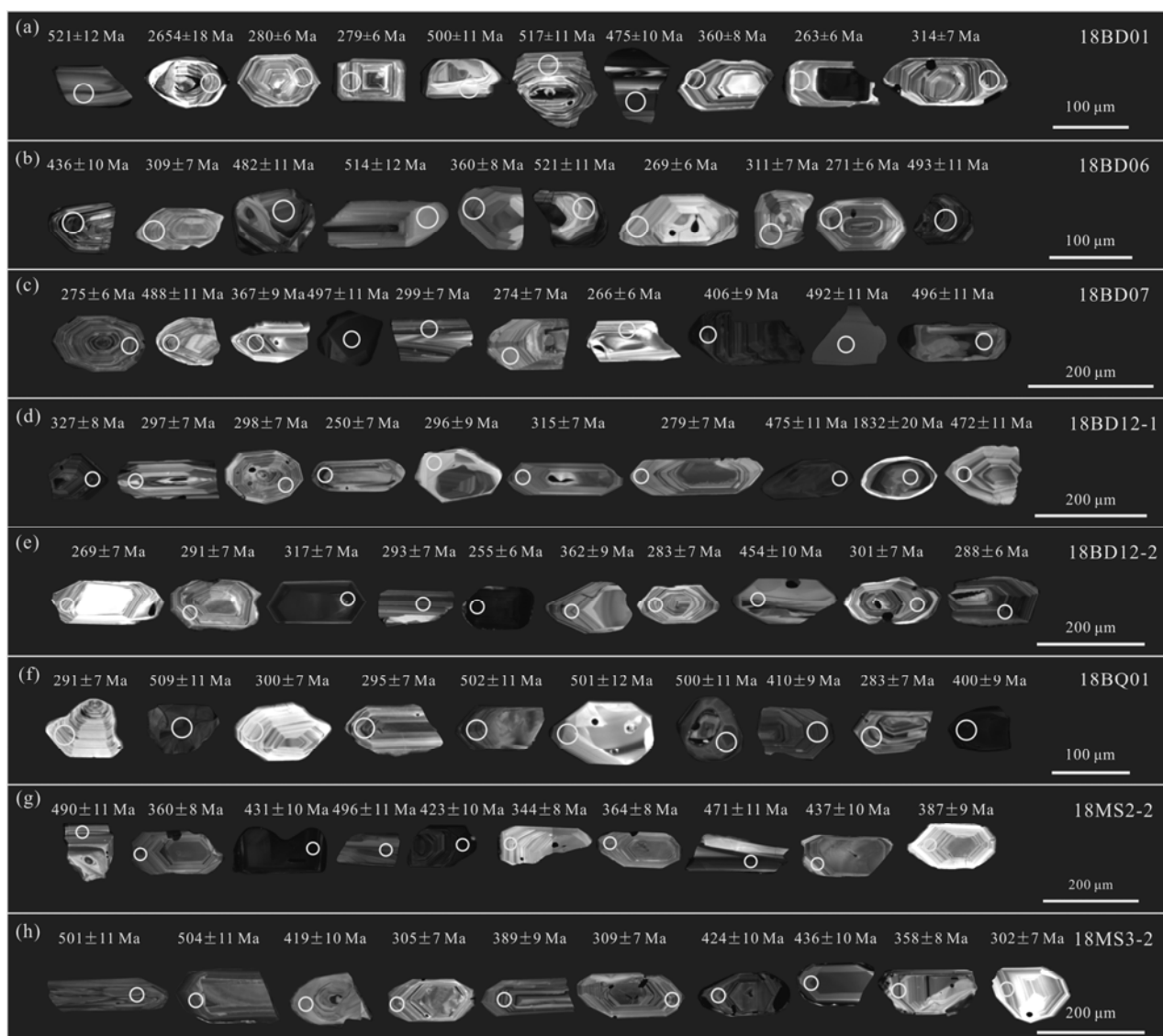


Fig. 4. Cathodoluminescence (CL) images of selected zircons from 8 samples in this study. Circles indicate analytical sites.

results. The Th/U ratios range from 0.12 to 1.39. The weighted mean $^{206}\text{Pb}/^{238}\text{U}$ age of zircons <1.0 Ga is 281–904 Ma. There are three main Phanerozoic age peaks: 281–300 Ma ($n=31$), 399–410 Ma ($n=7$), 495–516 Ma ($n=17$). The weighted mean $^{206}\text{Pb}/^{207}\text{Pb}$ age of zircons >1.0 Ga ranges from 1008 to 1456 Ma. Particularly, sample 18BQ01 contains 3 metamorphic zircons of 509 ± 11 Ma, 400 ± 9 Ma and 409 ± 9 Ma.

5 Discussion

5.1 Depositional age

5.1.1 Middle-Late Permian strata in Songliao Block

The Early, Middle and Late Permian strata are well developed in Binxian and Wuchang, in the eastern part of Harbin. Most of them are scattered in the Early-Middle Jurassic granites and volcanic rocks (Wu et al., 2011; Xu et al., 2013; and references therein), which are widely distributed in this region. Each group was determined by

sporadic fossil records with poor spatial continuity and unclear contact relationship. Sample 18BD01 is collected from the Yangmugang Formation of the Lower Permian (actually, the Middle Permian), and its maximum depositional age should be 260 ± 6 Ma (the youngest detrital zircon age; Fig. 3a). In this study, no evidence about the existence of Early Permian strata has been obtained. The real stratigraphic age of Yangmugang Formation is equivalent to Middle Permian Tumenling Formation. Sample 18BD06 and 18BD07 are from the Tumenling Formation. The maximum depositional ages are 267 ± 6 Ma and 266 ± 6 Ma, respectively (Figs. 3b, 3c); There is definite fossil evidence for the age of Tumenling Formation (Wang et al., 2009b; Zheng et al., 2018). Sample 18BD12-1 and 18BD12-2 were collected from a fossil-recorded profile of the Upper Permian Hongshan Formation (Deng et al., 2009). The maximum depositional ages are 250 ± 7 Ma and 255 ± 6 Ma, respectively (Figs. 3d, 3e). In summary, the maximum depositional age reflected

by the Permian detrital zircons in the Songliao Block can basically correspond well with previous chronological division of these stratigraphic units.

5.1.2 Late Carboniferous-Early Permian Strata in Jiamusi Block

Late Paleozoic strata in Mishan area also have poor spatial continuity. According to the regional geological survey references, their age was verified from the Early Devonian to the Late Permian, and various chronological division schemes cannot be unified. The profile where sample 18MS2-2 and 18MS3-2 were collected in this paper has no fossil records and is located beneath the Late Permian strata. This unit is characterized by the alternating layers of medium-thick volcanoclastic rocks, lavas and sandstones which is similar with the regional Carboniferous terrestrial strata, possibly the Zhenzishan Formation or Guangqing Formation (HBGMR, 1993). The maximum depositional age of sample 18MS2-2 and 18MS3-2 are 339 ± 8 Ma and 302 ± 7 Ma, which limits the depositional ages to the Early Carboniferous and Late Carboniferous (Figs. 3g, 3h), respectively, different from the stratigraphic ages defined previously. Sample 18BQ01 comes from the sandstone of Lower Permian Tatouhe Formation. The maximum depositional age of sample 18BQ01 is 281 ± 6 Ma (Fig. 3f), which is in the Early Permian and corresponds to the stratigraphic age defined before.

5.2 Provenance analysis

5.2.1 Significance of ~500 Ma age peak

The magmatic, metamorphic events with the age of ~500 Ma are widely distributed in the Jiamusi Block. Mashan Complex is a suite of Khondalite with clockwise P-T-t paths, whose metamorphic facies reach to granulite facies, including granulite, gneiss and metamorphic mudstone (Cao et al., 1992; Wilde et al., 1999). The Mashan Complex has an important metamorphic age peak of 500–530 Ma (Wilde et al., 1997, 2000, 2003; Wu et al., 2001; Huang et al., 2009; Zhou et al., 2010a, b; Yang et al., 2014). Synchronous Cambrian granitoids were also widely distributed in Jiamusi Block, including Luobei granodiorite (493 ± 4 Ma; Chen et al., 2018) in the north, Yilan granitic gneiss (492 ± 6 Ma; Han et al., 2019), Boli gneissic granite (476–530 Ma; Yang et al., 2018), Huanan gneissic granite (520.6 ± 2.8 Ma; Hao et al., 2018) in the middle segment, Mishan monzonitic granite and quartz syenite (500–516 Ma; Yang et al., 2014), Ximashan garnet granite (~500 Ma; Wilde et al., 2000) and monzonitic granite (510–535 Ma; Wilde et al., 2003) in the south.

But the corresponding metamorphic events of this age peak have not been reported in the Songliao Block. Although a small amount of Cambrian igneous rocks has been reported in the eastern margin of the Songliao Block, including Dongfengshan quartz monzonite (508 Ma, Liu et al., 2008; 523 Ma, Wutiepu et al., 2017) and Xigou granodiorite to the south of Yilan (captured zircon age of 525 Ma, Wang et al., 2017). These samples are too close to the Mudanjiang suture zone so it is a controversial issue whether they belong to the basement of Songliao Block or the Jiamusi Block which wedged westward into

Zhangguangcai Range due to orogenesis (Shao et al., 2013).

Our result show that the Middle Permian and pre-Permian strata but not Late Permian strata on both of Songliao and Jiamusi blocks have the age peak of ~500 Ma (Fig. 5, 6). We believe that the Jiamusi Block is the only stable source area of the ~500 Ma age peak. Therefore, the Songliao Block had received the detritus from the Jiamusi Block in and before Middle Permian, indicating that the Songliao and Jiamusi blocks have been connected in the time.

5.2.2 Significance of ~420–440 Ma age peak

There is another distinct age peak of ~420–440 Ma in the Carboniferous stratum (sample 18MS2-2; 18MS3-2; Figs. 3g, 3h) from Jiamusi Block. But no Silurian magmatic or metamorphic events have been reported in Jiamusi Block (Fig. 6), however, Silurian magmatic arcs, including Na-rich tonalite (426 Ma) of active continental margin property, calc-alkaline basalts (420 Ma), calc-alkaline granodiorite-monzonite and dacite (~435 Ma; Wang et al., 2017) and peraluminous monzonitic granite (~425 Ma; Wang et al., 2012) are developed in the southeastern margin of Zhangguangcai Range in Songliao Block. Therefore, the Songliao Block has provided the detritus for the terrestrial basin on Jiamusi Block during Carboniferous, indicating the two blocks had been connected during Carboniferous.

5.2.3 Significance of other age peaks

All samples have a small amount of Ordovician (~482–450 Ma) age (Figs. 5, 6), which can also roughly correspond to the magmatic events of the Ordovician active continental margin in Zhangguangcai Range. This magmatic arc is a series of medium-high potassic calc-alkaline intermediate-acid igneous rocks, including potassic monzonitic granite (475–461 Ma; Wang et al., 2017) in the middle of Zhangguangcai Range, rhyolite and A-type granite (460–450 Ma; Wang et al., 2012) in the Lesser Xing'an Range area.

The age peak of ~300 Ma from Permian sediments in Songliao Block corresponds well to the volcanic rocks, Tangjiatun Formation, of the Late Carboniferous in Songliao Block (Hao et al., 2014; Wang X et al., 2016), and there is also a small age peak (3 points) of ~300 Ma in 18MS3-2 from Jiamusi Block (Fig. 6). For the age peak of ~340–360 Ma in Jiamusi Block, it is consistent with a single data from Yanshou area in Songliao Block (366 Ma, A-type granite; Guo et al., 2018). The most prominent ~280–260 Ma age peak in the Permian strata corresponds to the Permian magmatic arc widely developed (Wu et al., 2001; Huang et al., 2008; Wei et al., 2012; Yu et al., 2013; Bi et al., 2016, 2017; Dong et al., 2017a, b) along the boundary between Songliao and Jiamusi Blocks.

In summary, the age peaks from the Carboniferous and Early Permian stratum in the Jiamusi Block, the most significant peak of ~420–440 Ma and the slightly smaller peak of ~482–450 Ma and ~300 Ma, are all correspond to the Paleozoic magmatism in the Songliao Block (Figs. 5, 6). Meanwhile, the prominent age peak of ~500 Ma from the Middle Permian stratum in the Songliao Block can

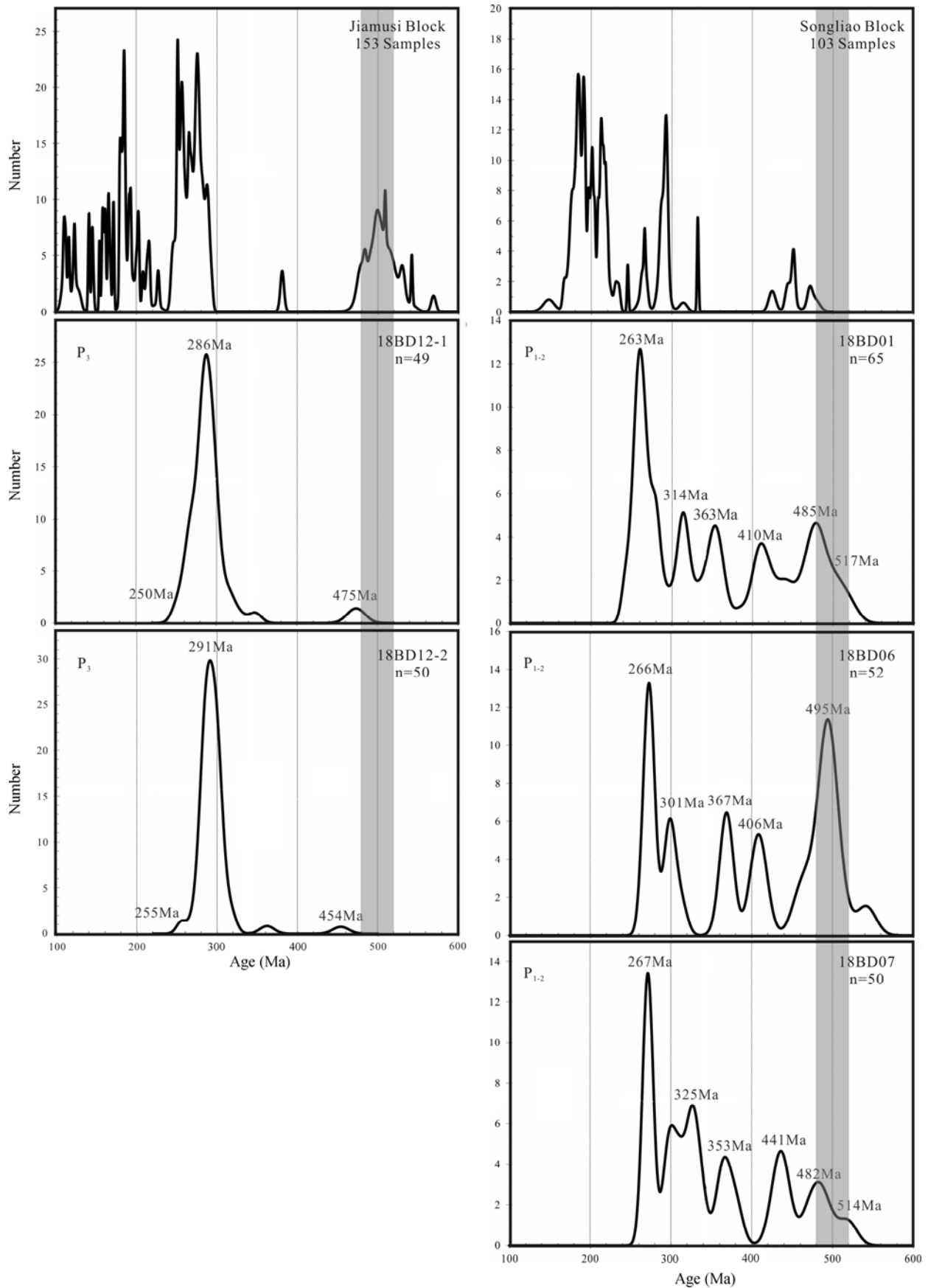


Fig. 5. Comparison of the zircon U-Pb age populations of Middle-Late Permian sandstones derived from Songliao Block, the upmost column is the statistical result of zircon U-Pb ages from igneous rocks in Songliao and Jiamusi Blocks.

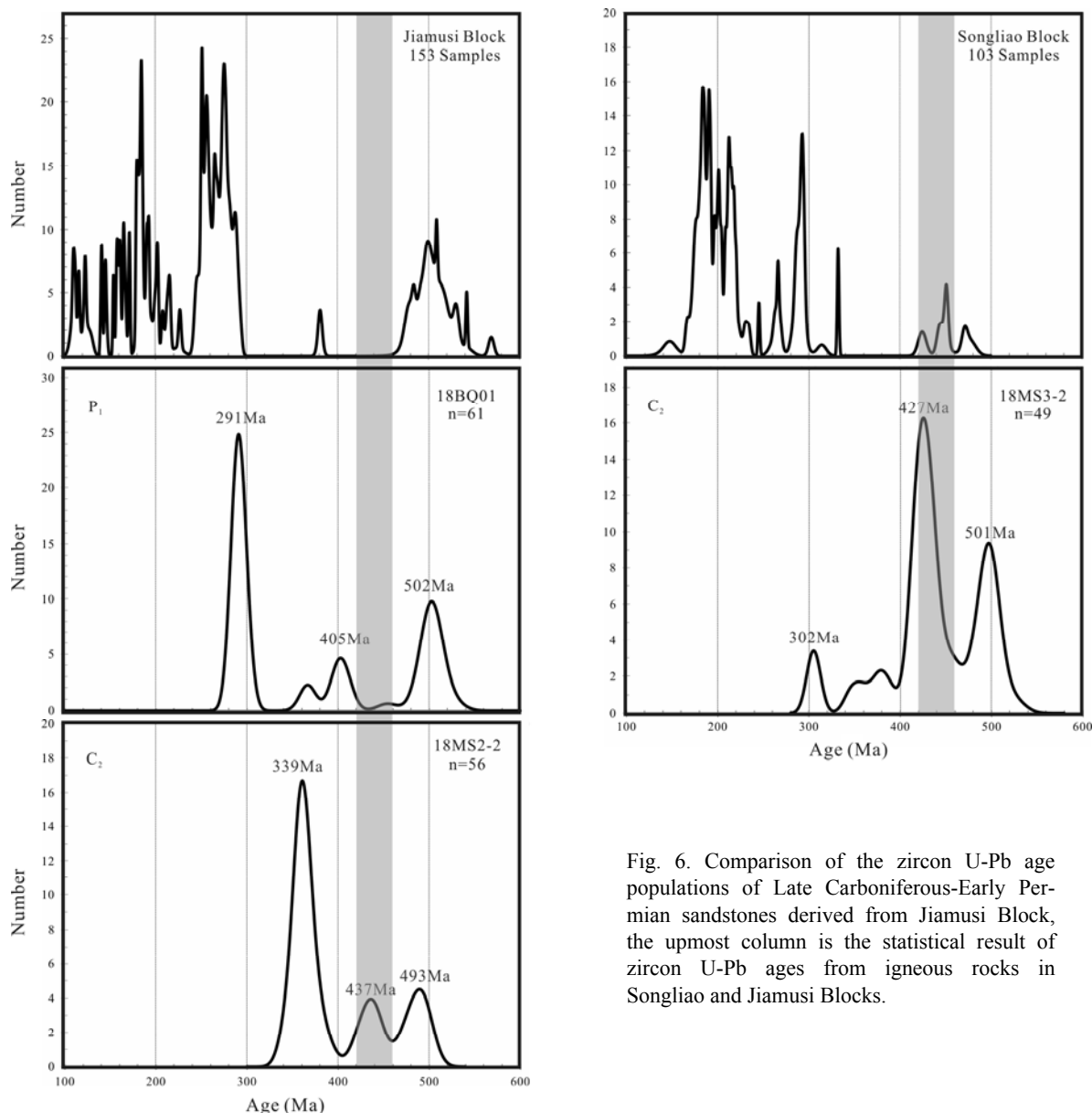


Fig. 6. Comparison of the zircon U-Pb age populations of Late Carboniferous-Early Permian sandstones derived from Jiamusi Block, the upmost column is the statistical result of zircon U-Pb ages from igneous rocks in Songliao and Jiamusi Blocks.

correspond to the Cambrian magmatism and metamorphism of the Jiamusi Block, which together illustrates that from the Carboniferous to the Middle Permian, the two blocks provided detritus for each other's terrestrial basins, showing the possibility that the two blocks had been integrated. Although the interval time is only ~10 Ma, most of the age peaks in the Songliao Block disappeared in the Late Permian except ~280 Ma, reflecting that during the transition from the Middle Permian to the Late Permian, the nature and provenance of the terrestrial basins in the eastern margin of the Songliao Block changed significantly, and the age peak of ~500 Ma from the Jiamusi Block was missing in the Songliao Block.

5.3 Paleozoic Tectonic Evolution History of Mudanjiang Suture Zone

In Zhangguangcai Range on the eastern margin of the

Songliao Block, there were reported syn- and post-orogenic granitoids whose age ranged from 480 to 420 Ma, representing the long-term subduction orogenesis along the Mudanjiang suture zone from Early Ordovician to Late Silurian. Igneous rocks in the eastern Zhangguangcai Range shows the characteristics of active continental margin environment during the Ordovician (Fig. 7a) (~482–450 Ma; Wang et al., 2016). The appearance of rhyolite (460–450 Ma; Wang et al., 2012) and A-type granite (471–479 Ma; Deng et al., 2018) in the Lesser Xing'an Range, which are relatively far from the subduction zone, suggest that the extensional environment similar to the back-arc basin appears in the western side of the subduction zone. Arc-related igneous rocks in Silurian, including quartz diorite (426 Ma), calc-alkaline basalt-andesite (420 Ma) and calc-alkaline granodiorite (~435 Ma), indicate that the oceanic crust subduction between the Songliao and Jiamusi blocks lasted until at least the

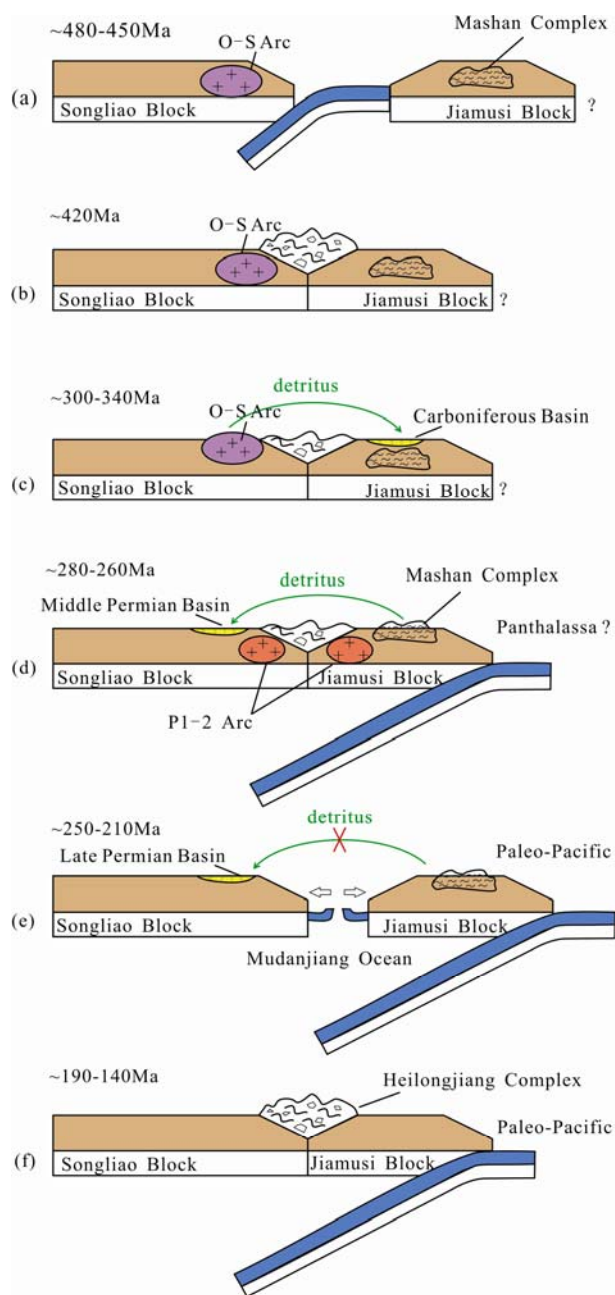


Fig. 7. Cartoon model for the tectonic evolution of Songliao and Jiamusi blocks during the Paleozoic to Mesozoic.

(a) the subduction between the Songliao and Jiamusi blocks started in ca. 480–450 Ma, as represented by the formation of early Paleozoic magmatic arc in Songliao Block; (b) the first amalgamation of the Songliao and Jiamusi blocks was completed in ca. 420 Ma; (c) the denudation of early Paleozoic magmatic arc made Songliao Block become the source area of the Carboniferous terrestrial basin in the Jiamusi Block; (d) the Mashan Complex also became the source area of the Permian terrestrial basin in the Songliao Block during ca. 280–260 Ma; (e) due to the subduction of the Paleo-Pacific, an intracontinental rifting was started along the former Mudanjiang-Yilan suture zone which made an interrupt of detritus transportation between the two blocks, formed a new limited oceanic basin as well as the Permian magmatic arc in ca. 250–210 Ma; (f) the final collision between the Songliao and Jiamusi blocks took place along the Mudanjiang-Yilan suture zone in ca. 190–140 Ma.

Late Silurian (Wang et al., 2016). The occurrence of collision-related peraluminous monzonitic granites in the

eastern middle section of Zhangguangcai Range indicates that the subduction has entered into terminal stage (Fig. 7b) (Wang et al., 2012). Besides, the Silurian metamorphic ages are also reported in the Cambrian granitoids in Jiamusi Block (Wen et al., 2008) and the amphibolites in the Heilongjiang Complex (Xie et al., 2008). The ~390 Ma bimodal volcanic rocks developed in the Jiamusi Block was interpreted as an extensional event combined with post-collision (Meng et al., 2011a).

Generally, age peaks of the terrestrial sediments in both Songliao and Jiamusi blocks should be comparable after their assemblage in the late Early Paleozoic. Age composition similarity of Devonian detrital zircons has been reported previously (Meng et al., 2010). The age peaks of 485–551 Ma in the Early Devonian strata in Songliao Block, Heilonggong Formation and Baoquan Formation (maximum depositional age are 403 Ma and 413 Ma, respectively), may come from the Jiamusi Block (Meng et al., 2010), and the Early-Middle Devonian Heitai Formation in the Jiamusi Block itself also has these age peaks (Meng et al., 2010; Li et al., 2019). As mentioned above, our study further confirmed the history that the two blocks shared the same source of detrital materials to each other from Carboniferous to Middle Permian (Figs. 7 c, 7d). Therefore, the Songliao and Jiamusi blocks were connected for a long time during the Late Paleozoic until the Middle Permian.

From Carboniferous to Permian, the sedimentary environment of Jiamusi Block and the eastern margin of Songliao Block were terrestrial facies, but eastward to the Russian Far East, re-entered into marine facies (Wang et al., 2008), indicating the existence of a long-term NE-trending uplifted terrain (probably an early Paleozoic orogenic belt) in the eastern part of the CAOB.

In the Mudanjiang suture zone, the existence of Heilongjiang Complex restricts an ocean which was closed in Mesozoic, i.e., the Mudanjiang Ocean. The minimum detrital zircons ages in meta-sedimentary rocks of Heilongjiang Complex includes several major groups: ~170–180 Ma, ~210 Ma and ~250 Ma (Zhou et al., 2009; Li et al., 2011; Zhu et al., 2017a, b, c; Dong et al., 2018a, b). The youngest metamorphic rock which protoliths are OIB igneous rocks yielded the age of ~140 Ma and ~180 Ma (Zhu et al., 2017a, b). Syntectonic mica Ar-Ar ages are distributed in ~140 Ma and ~160–180 Ma (Wu et al., 2007; Li et al., 2009, 2011; Aouizerat et al., 2019), these evidences limit the closure time of the Mudanjiang Ocean in the Middle Jurassic to Early Cretaceous. Ge et al. (2017) reported that the oldest MORB-type rock was the Late Permian and OIB-type rocks was the Early Permian. Our study above suggests that the Songliao and Jiamusi blocks were once amalgamated in the early Paleozoic, therefore, the Mudanjiang Ocean should be re-opened again sometime between Silurian and Jurassic, which is limited in not earlier than the Late Permian by our study (Fig. 7e). In addition, there are a few reports of Permian-Triassic bimodal volcanic rocks which also support the extension event during this period (Xu et al., 2009; Meng et al., 2011b; Wang et al., 2015).

The reopen of Mudanjiang Ocean temporally corresponds to the Middle-Late Permian magmatic arcs

widely distributed in the Songliao and Jiamusi blocks. Including: granite in Lesser Xing'an Range (266–259 Ma; Dong et al., 2017a), arc-related metagabbro at Luobei (267–264 Ma; Dong et al., 2018a) to the north, arc-related metagabbro at Yilan (256–259 Ma; Dong et al., 2017b), granitic gneiss at Boli (254–270 Ma; Wu et al., 2001), granite at Huanan (259–278 Ma; Huang et al., 2008; Dong et al., 2017a), I-type granite and bimodal igneous rocks at Baoqing (~260 Ma; Bi et al., 2016, 2017), I-type granite in the west of Mudanjiang (256–252 Ma; Yu et al., 2013) to the south. The subduction-related magmatic arcs on the two blocks may be related to the initial subduction of the Paleo-Pacific (Ge et al., 2018), which resulted in the back-arc extension and the second opening of the Mudanjiang Ocean.

In conclusion, our study gives more constraints to the tectonic evolution of Songliao and Jiamusi blocks during Paleozoic (Fig. 7): The Songliao and Jiamusi blocks completed their first assemblage in the Early Paleozoic (Wang et al., 2012; Wang et al., 2016; Liu et al., 2017), and remained as an united Block till the end of the Permian (Meng et al., 2010; Xu et al., 2012). At the end of Permian, due to the eastward subduction of Paleo-Pacific Ocean (Zhou et al., 2009; Sun et al., 2015; Yang et al., 2015, 2017; Bi et al., 2016, 2017), the Songliao-Jiamusi united Block was in a back-arc extension setting and broken up probably along the Paleozoic suture zone, resulting in the re-opening of the Mudanjiang Ocean. Due to the continuous subduction of the Paleo-Pacific Ocean, the short-lived Mudanjiang ocean was closed again in sometime between the Middle Jurassic and Early Cretaceous (Wu et al., 2007; Li et al., 2009, 2011; Zhu et al., 2017 a, b, c; Dong et al., 2018b).

6 Conclusions

(1) The maximum depositional age of Middle Permian Tumenling Formation in Songliao Block is ~260 Ma, that of Late Permian Hongshan Formation is ~250 Ma, and that of Early Permian Tatouhe Formation in Baoqing area in Jiamusi Block is ~290 Ma. These results support the previous stratigraphic age division scheme.

(2) The terrestrial basins of Songliao Block in the Middle Permian accepted the detrital materials from ~500 Ma source area in the Jiamusi Block, and the Jiamusi Block in the Late Carboniferous-Early Permian accepted the detrital materials from the ~420–430 Ma source area in Zhangguangcai Range of Songliao Block, indicating that they might be connected in the Carboniferous to Middle Permian.

(3) From Middle Permian to Late Permian, the sedimentary basins of the Songliao Block experienced an important provenance change. The Jiamusi Block was no longer the source area of Songliao Block since at least the Late Permian, i.e., there had a paleogeographic isolation between the two blocks. The Mudanjiang Ocean basin may have been opened.

Acknowledgement

This study was supported by the National Key R&D

Plan of China (Grant No. 2017YFC0601300–01), 973 Program (Grant 2013CB429802), NSFC (Grant 41302175, 41502207). We thanks the editors for their helpful text editing.

Manuscript received May 15, 2019

accepted Aug. 14, 2019

associate EIC XIAO Wenjian

edited by LIU Lian

References

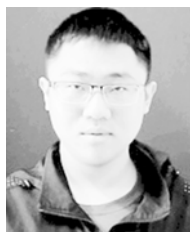
- Andersen, T., 2005. Detrital zircons as tracers of sedimentary provenance: Limiting conditions from statistics and numerical simulation. *Chemical Geology*, 216(3–4): 249–270.
- Aouizerat, A., Xiao, W.J., Schulmann, K., Jeřábek, P., Monié, P., Zhou, J.B., Zhang, J.J., Ao, S.J., Li, R., Li, Y.C., and Esmacili, R., 2019. Structures, strain analyses, and $^{40}\text{Ar}/^{39}\text{Ar}$ ages of blueschist-bearing Heilongjiang Complex (NE China): Implications for the Mesozoic tectonic evolution of NE China. *Geological Journal*, 54(2): 716–745.
- Bai, J.W., Wang, W.X., and Zhang, H.R., 1988. Character of glaucophane schists in metamorphic zone in Yilan, Mudanjiang, Heilongjiang. *Acta Petrologica et Mineralogica*, 7(4): 298–308 (in Chinese with English abstract).
- Bi, J.H., Ge, W.C., Yang, H., Wang, Z.H., Xu, W.L., Yang, J.H., Xing, D.H., and Chen, H.J., 2016. Geochronology and geochemistry of late Carboniferous-middle Permian I-and A-type granites and gabbro-diorites in the eastern Jiamusi Massif, NE China: Implications for petrogenesis and tectonic setting. *Lithos*, 266: 213–232.
- Bi, J.H., Ge, W.C., Yang, H., Wang, Z.H., Dong, Y., Liu, X.W., and Ji, Z., 2017. Age, petrogenesis, and tectonic setting of the Permian bimodal volcanic rocks in the eastern Jiamusi Massif, NE China. *Journal of Asian Earth Sciences*, 134: 160–175.
- Blank, L.P., Kamo, S.L., Williams, I.S., Mundil, R., Davis, D.W., Korsch, R.J., and Foudoulis, C., 2003. The application of SHRIMP to Phanerozoic geochronology: A critical appraisal of four zircon standards. *Chemical Geology*, 200(1–2): 171–188.
- Chen, X., Liu J.J., Carranza, E.J., Zhang, D.H., Collins, A.S., Yang, B., Xu, B.W., Zhai, D.G., Wang, Y.H., Wang, J.P., and Liu, Z.J., 2019. Geology, geochemistry, and geochronology of the Cuihongshan Fe-polymetallic deposit, Heilongjiang Province, NE China. *Geological Journal*, 54(3): 1254–1278.
- Deng, C.Z., Sun, D.Y., Sun, G.Y., Lv, C.L., Qin, Z., Ping, X.Q., and Li, G.H., 2018. Age and geochemistry of Early Ordovician A-type granites in the Northeastern Songnen Block, NE China. *Acta Geochimica*, 37(6): 805–819.
- Deng, S.H., Wan, C.B., and Yang, J.G., 2009. Discovery of a Late Permian Angara-Cathaysia mixed flora from Acheng of Heilongjiang, China, with discussions on the closure of the Paleo-Asian Ocean. *Science in China Series D-Earth Sciences*, 52(11): 1746–1755 (in Chinese with English abstract).
- Dong, Y., Ge, W.C., Yang, H., Bi, J.H., Wang, Z.H., and Xu, W.L., 2017a. Permian tectonic evolution of the Mudanjiang Ocean: Evidence from zircon U-Pb-Hf isotopes and geochemistry of a N-S trending granitoid belt in the Jiamusi Massif, NE China. *Gondwana Research*, 49: 147–163.
- Dong, Y., Ge, W.C., Yang, H., Xu, W.L., Bi, J.H., and Wang, Z.H., 2017b. Geochemistry and geochronology of the Late Permian mafic intrusions along the boundary area of Jiamusi and Songnen-Zhangguangcai Range massifs and adjacent regions, northeastern China: Petrogenesis and implications for the tectonic evolution of the Mudanjiang Ocean. *Tectonophysics*, 694: 356–367.
- Dong, Y., He, Z.H., Ren, Z.H., Ge, W.C., Yang, H., Ji, Z., and He, Y., 2018a. Formation of the Permian Taipinggou igneous rocks, north of Luobei (Northeast China): implications for the subduction of the Mudanjiang Ocean beneath the Bureya-Jiamusi Massif. *International Geology Review*, 60(10): 1195–1212.
- Dong, Y., Ge, W.C., Yang, H., Ji, Z., He, Y., Zhao, D., and Xu,

- W.L., 2018b. Convergence history of the Jiamusi and Songnen-Zhangguangcai Range massifs: Insights from detrital zircon U-Pb geochronology of the Yilan Heilongjiang Complex, NE China. *Gondwana Research*, 56: 51–68.
- Feng, Z.Q., Liu, Y.J., Liu, B.Q., Wen, Q.B., Li, W.M., and Liu, Q., 2016. Timing and nature of the Xinlin-Xiguitu Ocean: constraints from ophiolitic gabbros in the northern Great Xing'an Range, eastern Central Asian Orogenic Belt. *International Journal of Earth Sciences*, 105(2): 491–505.
- Gehrels, G., 2011. Detrital zircon U - Pb geochronology: Current methods and new opportunities. In: Busby C, Pérez A A (eds.). *Tectonics of sedimentary basins: Recent advances*. John Wiley & Sons, 45–62.
- Ge, M.H., Zhang, J.J., Li, L., Liu, K., Ling, Y.Y., Wang, J.M., and Wang, M., 2017. Geochronology and geochemistry of the Heilongjiang Complex and the granitoids from the Lesser Xing'an-Zhangguangcai Range: Implications for the late Paleozoic-Mesozoic tectonics of eastern NE China. *Tectonophysics*, 717: 565–584.
- Ge, M.H., Zhang, J.J., Li, L., and Liu, K., 2018. A Triassic-Jurassic westward scissor-like subduction history of the Mudanjiang Ocean and amalgamation of the Jiamusi Block in NE China: Constraints from whole-rock geochemistry and zircon U-Pb and Lu-Hf isotopes of the Lesser Xing'an-Zhangguangcai Range granitoids. *Lithos*, 302, 263–277.
- Ge, W.C., Wu, F.Y., Zhou, C.Y., and Rahman, A.A., 2005. Emplacement age of the Tahe granite and its constraints on the tectonic nature of the Erguna block in the northern part of the Da Xing'an Range. *Chinese Science Bulletin* 50, 2097–2105 (in Chinese with English abstract).
- Guo, P., Xu, W.L., Wang, Z.W., Wang, F., and Luan, J.P., 2018. Geochronology and geochemistry of Late Devonian-Carboniferous igneous rocks in the Songnen-Zhangguangcai Range Massif, NE China: Constraints on the late Paleozoic tectonic evolution of the eastern Central Asian Orogenic Belt. *Gondwana Research*, 57: 119–132.
- Han, W., Zhou, J.B., Wilde, S.A., and Li, L., 2019. LA - ICPMS zircon U-Pb dating of the Heilongjiang Complex in the Luobei area: New constraints for the late Palaeozoic - Mesozoic tectonic evolution of Jiamusi Block, NE China. *Geological Journal*, doi: 10.1002/gj.3443.
- Hao, Y.J., Ren, Y.S., Zhao, H.L., Lai, K., Zhao, X., and Ma, Y.P., 2018. Metallogenic mechanism and tectonic setting of Tungsten mineralization in the Yangbishan deposit in Northeastern China. *Acta Geologica Sinica (English Edition)*, 92(1): 241–267.
- Hao, W.L., Xu, W.L., Wang, F., Tang, J., Xu, M.J. and Gao, F.H., 2014. Geochronology of the “Neoproterozoic” Yimianpo Group in the Zhangguangcai Range, NE China: Constraints from U-Pb ages of detrital and magmatic zircons. *Acta Petrologica Sinica*, 30(7): 1867–1878 (in Chinese with English abstract).
- HGBMR (Heilongjiang Bureau of Geology and Mineral Resources), 1993. *Regional Geology of Heilongjiang Province*. Beijing: Geological Publishing House, 347–418 (in Chinese).
- Huang, Y.C., Ren, D.H., Zhang, X.Z., Xiong, X.S., Zhang, C.Y., Wang, Y., and Zhao, L.L., 2008. Zircon U-Pb dating of the Meizuo granite and geological significance in the Huanan uplift, east Heilongjiang Province. *Journal of Jilin University (Earth Science Edition)*, 38(4): 631–638 (in Chinese with English Abstract).
- Huang, Y.C., Zhang, X.Z., Zhang, H.B., Xiong, X.S., Liu, C.L., and Zhao, L.L., 2009. Geochemical characteristics and sedimentation age of the Maji jie Group in Eastern Heilongjiang Province, China. *Acta Geologica Sinica* 83(2): 295–303 (in Chinese with English Abstract).
- Jian, P., Liu, D.Y., Kröner, A., Windley, B.F., Shi, Y.R., Zhang, F.Q., Shi, G.H., Miao, L.C., Zhang, W., Zhang, Q., Zhang, L.Q., and Ren, J.S., 2008. Time scale of an early to mid-Paleozoic orogenic cycle of the long-lived Central Asian Orogenic Belt, Inner Mongolia of China: implications for continental growth. *Lithos*, 101(3–4): 233–259.
- Li, G.Y., Zhou, J.B., Wilde, S.A., and Li, L., 2019. The transition from a passive to an active continental margin in the Jiamusi Block: Constraints from Late Paleozoic sedimentary rocks. *Journal of Geodynamics*, 129: 131–148.
- Li, J.Y., 2006. Permian geodynamic setting of Northeast China and adjacent regions: closure of the Paleo-Asian Ocean and subduction of the Paleo-Pacific Plate. *Journal of Asian Earth Sciences*, 26(3–4): 207–224.
- Li, R.S., 1991. Xinlin Ophiolite. *Heilongjiang Geology*, 2, 19–31 (in Chinese with English abstract).
- Li, W.M., Takasu, A., Liu, Y.J., Genser, J., Neubauer, F., and Guo, X.Z., 2009. $^{40}\text{Ar}/^{39}\text{Ar}$ ages of the high-P/T metamorphic rocks of the Heilongjiang Complex in the Jiamusi Massif, northeastern China. *Journal of Mineralogical and Petrological Sciences*, 104: 110–116.
- Li, W.M., Takasu, A., Liu, Y.J., and Guo, X.Z., 2010. Newly discovered garnet-barroisite schists from the Heilongjiang Complex in the Jiamusi Massif, northeastern China. *Journal of Mineralogical and Petrological Sciences*, 105: 86–91.
- Li, W.M., Takasu, A., Liu, Y.J., Genser, J., Zhao, Y.L., Han, G.Q., and Guo, X.Z., 2011. U-Pb and $^{40}\text{Ar}/^{39}\text{Ar}$ age constrains on protolith and high-P/T type metamorphism of the Heilongjiang Complex in the Jiamusi Massif, NE China. *Journal of Mineralogical and Petrological Sciences*, 106(6): 326–331.
- Li, W.M., Liu, Y.J., Takasu, A., Zhao, Y.L., Wen, Q.B., Guo, X.Z., and Zhang, L., 2014. Pressure(P)-temperature (T)-time (t) paths of the blueschists from the Yilan area, Heilongjiang Province. *Acta Petrologica Sinica*, 30(10): 3085–3099 (in Chinese with English abstract).
- Liu, J.F., Chi, X.G., Dong, C.Y., Zhao, Z., Li, G.R., and Zhao, Y.D., 2008. Discovery of Early Paleozoic granites in the eastern Xiao Hinggan Mountains, northeastern China and their tectonic significance. *Geological Bulletin of China*, 27(4): 534–544 (in Chinese with English abstract).
- Liu, Y.J., Zhang, X.Z., Jin, W., Chi, X.G., Wang, C.W., Ma, Z.H., Han, G.Q., Wen, Q.B., Zhao, Y.L., Wang, W.D., and Zhao, X.F., 2010. Late Paleozoic tectonics evolution in Northeast China. *Geology in China*, 37: 943–951 (in Chinese with English abstract).
- Liu, Y.J., Li, W.M., Feng, Z.Q., Wen, Q.B., Neubauer, F., and Liang, C.Y., 2017. A review of the Paleozoic tectonics in the eastern part of Central Asian Orogenic Belt. *Gondwana Research*, 43: 123–148.
- Luan, J.P., Xu, W.L., Wang, F., Wang, Z.W., and Guo, P., 2017. Age and geochemistry of Neoproterozoic granitoids in the Songnen-Zhangguangcai Range Massif, NE China: Petrogenesis and tectonic implications. *Journal of Asian Earth Sciences*, 148: 265–276.
- Ludwig, K.R., 2012. *Isoplot/Ex rev. 3.75—A Geochronological Toolkit for Microsoft Excel*. Berkeley Geochronology Center Special Publication, No. 5, 75p.
- Meng, E., Xu, W.L., Pei, F.P., Yang, D.B., Yu, Y., and Zhang, X.Z., 2010. Detrital-zircon geochronology of Late Paleozoic sedimentary rocks in eastern Heilongjiang Province, NE China: implications for the tectonic evolution of the eastern segment of the Central Asian Orogenic Belt. *Tectonophysics*, 485: 42–51.
- Meng, E., Xu W.L., Pei F.P., and Wang, F., 2011a. Middle Devonian volcanism in eastern Heilongjiang Province and its tectonic implications: constraints from petro-geochemistry, zircon U-Pb chronology and Sr-Nd-Hf isotopes. *Acta Petrologica et Mineralogica*, 30(5): 883–900 (in Chinese with English abstract).
- Meng, E., Xu W.L., Pei F.P., Yang, D.B., Wang, F., and Zhang, X.Z., 2011b. Permian bimodal volcanism in the Zhangguangcai Range of eastern Heilongjiang Province, NE China: zircon U-Pb-Hf isotopes and geochemical evidence. *Journal of Asian Earth Sciences*, 41(2): 119–132.
- Quan, J.Y., Chi, X.G., Zhang, R., Sun, W., Fan, L.F., and Hu, Z.C., 2013. LA-ICP-MS U-Pb geochronology of detrital zircon from the Neoproterozoic Dongfengshan Group in Songnen Massif and its geological significance. *Geological Bulletin of China*, 32(2/3): 353–364 (in Chinese with English abstract).
- Sengör, A.C., Natal'in, B.A., and Burtman, V.S., 1993. Evolution of the Altaid tectonic collage and Palaeozoic crustal

- growth in Eurasia. *Nature*, 364(6435): 299–307.
- Shao, J.A., Li, Y.F., and Tang, K.D., 2013. Restoration of the orogenic processes of Zhangguangcai Range. *Acta Petrologica Sinica*, 29(9): 2959–2970 (in Chinese with English abstract).
- Sun, M.D., Xu, Y. G., Wilde, S.A., Chen, H.L., and Yang, S.F., 2015. The Permian Dongfanghong island-arc gabbro of the Wandashan Orogen, NE China: Implications for Paleo-Pacific subduction. *Tectonophysics*, 659: 122–136.
- Wang, C.W., Jin, W., Zhang, X.Z., Ma, Z.H., Chi, X.G., Liu, Y.J., and Li, N., 2008. New understanding of the late Paleozoic tectonics in northeastern China and adjacent areas. *Journal of Stratigraphy*, 32: 119–136 (in Chinese with English abstract).
- Wang, C.W., Sun, Y.W., Li, N., Liu, H., and Zhao, G.W., 2009a. On the distribution of Late Paleozoic strata in northeast China. *Journal of Stratigraphy*, 33(1): 56–61 (in Chinese with English abstract).
- Wang, C.W., Sun, Y.W., Li, N., Zhao, G.W., and Ma, X.Q., 2009b. Tectonic implications of Late Paleozoic stratigraphic distribution in Northeast China and adjacent region. *Science in China Series D-Earth Sciences*, 52(5): 619–626.
- Wang, F., Xu, W.L., Meng, E., Cao, H.H., and Gao, F.H., 2012. Early Paleozoic amalgamation of the Songnen-Zhangguangcai Range and Jiamusi massifs in the eastern segment of the Central Asian Orogenic Belt: geochronological and geochemical evidence from granitoids and rhyolites. *Journal of Asian Earth Sciences*, 49: 234–248.
- Wang, F., Xu, W.L., Gao, F.H., Zhang, H.H., Pei, F.P., Zhao, L., and Yang, Y., 2014. Precambrian terrane within the Songnen-Zhangguangcai Range Massif, NE China: Evidence from U-Pb ages of detrital zircons from the Dongfengshan and Tadong Groups. *Gondwana Research*, 26(1): 402–413.
- Wang, F., Xu, W.L., Xu, Y.G., Gao, F.H., and Ge, W.C., 2015. Late Triassic bimodal igneous rocks in eastern Heilongjiang Province, NE China: implications for the initiation of subduction of the Paleo-Pacific Plate beneath Eurasia. *Journal of Asian Earth Sciences*, 97: 406–423.
- Wang, X., Zheng, T., Gu, H.J., Niu, Y.H., and Liang, C.Z., 2016. The U-Pb chronological evidence for the volcanic rocks of Tangjiatun Formation in east Harbin, Heilongjiang Province. *Geology and Resources*, 25(3): 237–243 (in Chinese with English abstract).
- Wang, Z.W., Xu, W.L., Pei, F.P., Wang, F., and Guo, P., 2016. Geochronology and geochemistry of early Paleozoic igneous rocks of the Lesser Xing'an Range, NE China: implications for the tectonic evolution of the eastern Central Asian Orogenic Belt. *Lithos*, 261: 144–163.
- Wang Z.W., Xu, W.L., Pei, F.P., Guo, P., Wang, F., and Li, Y., 2017. Geochronology and geochemistry of early Paleozoic igneous rocks from the Zhangguangcai Range, northeastern China: Constraints on tectonic evolution of the eastern Central Asian Orogenic Belt. *Lithosphere*, 9(5): 803–827.
- Wei, H.Y., Sun, D.Y., Ye, S.Q., Yang, Y.C., Liu, Z.H., Liu, X.M., and Hu, Z.C., 2012. Zircon U-Pb ages and its geological significance of the granitic rocks in the Yichun-Hegang region, southeastern Xiao Hinggan Mountains. *Earth Science-Journal of China University of Geosciences*, 37: 50–59 (in Chinese with English abstract).
- Wen, Q.B., Liu, Y.J., Gao, F., Xu, M., Li, W.M., Feng, Z.Q., Zhou, J.P. and Liang, C.Y., 2017. Thermochronological evidence for multi-phase uplifting and exhumation history the Jiamusi uplift in eastern Heilongjiang, China. *Acta Petrologica Sinica*, 33(6): 1789–1804 (in Chinese with English abstract).
- Wilde, S.A., 1997. The identification of a Late Pan-African granulite facies event in Northeastern China: SHRIMP U-Pb zircon dating of the Mashan Group at Liu Mao, Heilongjiang Province, China. *Beijing: Proceedings of the 30th IGC*, 17: 59–74.
- Wilde, S.A., Dorsett-Bain, H.L., and Lennon, R.G., 1999. Geological setting and controls on the development of graphite, sillimanite and phosphate mineralization within the Jiamusi Massif: an exotic fragment of Gondwanaland located in North-Eastern China. *Gondwana Research*, 2: 21–46.
- Wilde, S.A., Zhang, X.Z., and Wu, F.Y., 2000. Extension of a newly-identified 500Ma metamorphic terrain in Northeast China: further U-Pb SHRIMP dating of the Mashan Complex, Heilongjiang Province, China. *Tectonophysics*, 328: 115–130.
- Wilde, S.A., Wu, F.Y., and Zhang, X.Z., 2003. Late Pan-African magmatism in Northeastern China: SHRIMP U-Pb zircon evidence for igneous ages from the Mashan Complex. *Precambrian Research*, 122: 311–327.
- Wilde, S.A., and Zhou, J.B., 2015. The late Paleozoic to Mesozoic evolution of the eastern margin of the Central Asian Orogenic Belt in China. *Journal of Asian Earth Sciences*, 113: 909–921.
- Wu, Y.B., and Zheng, Y.F., 2004. The study on the zircon genesis mineralogy and its impacts on the interpretation of U-Pb age restriction. *Chinese Science Bulletin*, 49: 1554–1569 (in Chinese with English abstract).
- Wu, F.Y., Wilde, S.A., and Sun, D.Y., 2001. Zircon SHRIMP ages of gneissic granites in Jiamusi Massif, northeastern China. *Acta Petrologica Sinica*, 17: 443–452 (in Chinese with English abstract).
- Wu, F.Y., Yang, J.H., Lo, C.H., Wilde, S.A., Sun, D.Y., and Jahn, B.M., 2007. The Heilongjiang Group: a Jurassic accretionary complex in the Jiamusi Massif at the western Pacific margin of northeastern China. *Island Arc*, 16: 156–172.
- Wu, F.Y., Sun, D.Y., Ge, W.C., Zhang, Y.B., Grant, M.L., Wilde, S.A., and Jahn, B.M., 2011. Geochronology of the Phanerozoic granitoids in northeastern China. *Journal of Asian Earth Sciences*, 41: 1–30.
- Wutiepu, W., Yang, Y.C., Tan, Y., Han, S.Z., Guo, Y.F., Wang, Q.S., Wang, X.Y., and Wang, F.B., 2018. Geochemistry, geochronology, and geological implications of the granitoids associated with the Dongfengshan gold deposit, Heilongjiang Province, NE China. *Geological Journal*, 53(5): 2143–2160.
- Xiao, W.J., Windley, B.F., Hao, J., and Zhai, M.G., 2003. Accretion leading to collision and the Permian Solonker suture, Inner Mongolia, China: Termination of the central Asian orogenic belt. *Tectonics*, 22(6).
- Xie, H.Q., Zhang, F.Q., Miao, L.C., Chen, F.K., and Liu, D.Y., 2008. Zircon SHRIMP U-Pb dating of the amphibolite from “Heilongjiang Group” and the granite in Mudanjiang area, NE China, and its geological significance. *Acta Petrologica Sinica*, 24(6): 1237–1250 (in Chinese with English abstract).
- Xu, B., Zhao, P., Wang, Y.Y., Liao, W., Luo, Z.W. Bao, Q.Z., and Zhou, Y.H., 2015. The pre-Devonian tectonic framework of Xing'an-Mongolia orogenic belt (XMOB) in north China. *Journal of Asian Earth Sciences*, 97: 183–196.
- Xu, W.L., Ji, W.Q., Pei F.P., Meng, E., Yu, Y., Yang, D.B., and Zhang, X.Z., 2009. Triassic volcanism in eastern Heilongjiang and Jilin provinces, NE China: Chronology, geochemistry, and tectonic implications. *Journal of Asian Earth Sciences*, 34 (3): 392–402.
- Xu, W.L., Wang, F., Meng, E., Gao, F.H., Pei, F.P., Yu, J.J., and Tang, J., 2012. Paleozoic-Early Mesozoic Tectonic Evolution in the Eastern Heilongjiang Province, NE China: evidence from Igneous Rock Association and U-Pb Geochronology of Detrital Zircons. *Journal of Jilin University (Earth Science Edition)*, 42(5): 1378–1389 (in Chinese with English abstract).
- Xu, W.L., Pei, F.P., Wang, F., Meng, E., Ji, W.Q., Yang, D.B., and Wang, W., 2013. Spatial-temporal Relationships of Mesozoic Volcanic Rocks in NE China: constraints on Tectonic Overprinting and Transformations Between Multiple Tectonic Regimes. *Journal of Asian Earth Sciences*, 74: 167–193.
- Yang, H., Ge, W.C., Zhao, G.C., Dong, Y., Bi, J.H., Wang, Z.H., Yu, J.J., and Zhang, Y.L., 2014. Geochronology and geochemistry of Late Pan-African intrusive rocks in the Jiamusi-Khanka Block, NE China: petrogenesis and geodynamic implications. *Lithos*, 208: 220–236.
- Yang, H., Ge, W.C., Zhao, G.C., Yu, J.J., and Zhang, Y.L., 2015. Early Permian-Late Triassic granitic magmatism in the Jiamusi-Khanka Massif, eastern segment of the Central Asian Orogenic Belt and its implications. *Gondwana Research*, 27 (4): 1509–1533.
- Yang, H., Ge, W.C., Dong, Y., Bi, J.H., Wang, Z.H., and Ji, Z., 2017. Record of Permian-Early Triassic continental arc

- magmatism in the western margin of the Jiamusi Block, NE China: petrogenesis and implications for Paleo-Pacific subduction. *International Journal of Earth Sciences*, 106(6): 1919–1942.
- Yang, H., Ge, W.C., Bi, J.H., Wang, Z.H., Tian, D.X., Dong, Y., and Chen, H.J., 2018. The Neoproterozoic-early Paleozoic evolution of the Jiamusi Block, NE China and its East Gondwana connection: Geochemical and zircon U-Pb-Hf isotopic constraints from the Mashan Complex. *Gondwana Research*, 54: 102–121.
- Ye, H.W., Zhang, X.Z., and Zhou, Y.W., 1994. The texture and evolution of Manzhouli-Suifenhe lithosphere—Study based on features of blueschist and ophiolites. In: M-SGT Geology Group (eds.), *Geological Studies of Lithospheric Structure and Evolution of Manzhouli-Suifenhe Geotranssect, China*. Beijing: Seismic Press, 73–83 (in Chinese with English abstract).
- Yu, J.J., Wang, F., Xu, W.L., Gao, F.H., and Tang, J., 2013. Late Permian tectonic evolution at the southeastern margin of the Songnen-Zhangguangcai Range Massif, NE China: Constraints from geochronology and geochemistry of granitoids. *Gondwana Research*, 24(2): 635–647.
- Zhang, X.Z., 1992. Heilongjiang mélange: the evidence of Caledonian suture zone of the Jiamusi massif. *Journal of Changchun University of Earth Sciences, Special Issue: Doctoral Thesis*, 22: 94–101 (in Chinese with English abstract).
- Zhang, X.Z., Yang, B.J., Wu, F.Y., and Liu, G.X., 2006. The lithosphere structure in the Hingmang-Jihe (Hingan-Mongolia-Heilongjiang) region, northeastern China. *Geology in China*, 33(4): 816–823 (in Chinese with English abstract).
- Zhang, X.Z., Ma, Y.X., Chi, X.G., Zhang, F.X., Sun, Y.W., Guo, Y., and Zeng, Z., 2012. Discussion on Phanerozoic tectonic evolution in northeastern China. *Journal of Jilin University (Earth Science Edition)*, 42(5): 1269–1285 (in Chinese with English abstract).
- Zhao, Y.L., Liu, Y.J., Li, W.M., Wen, Q.B., and Han, G.Q., 2010. High-pressure metamorphism in the Mudanjiang area, southern Jiamusi massif: petrological and geochronological characteristics of the Heilongjiang complex, China. *Geological Bulletin of China*, 29(2/3): 243–253 (in Chinese with English abstract).
- Zheng, Y.J., Huang, X., Sun, Y.W., Song, S.J., Chen, S.W., Zhang, J., Gong, F.H., Zhang, D.J., Zhang, H.H., and Su, F., 2018. The Carboniferous-Permian stratigraphic division and correlation in the Songliao Basin and its peripheral areas. *Geology and Resources*, 27(1): 1–15 (in Chinese with English abstract).
- Zhou, J.B., Wilde, S.A., Zhang, X.Z., Zhao, G.C., Zheng, C.Q., Wang, Y.J., and Zhang, X.H., 2009. The onset of Pacific margin accretion in NE China: evidence from the Heilongjiang high-pressure metamorphic belt. *Tectonophysics*, 478: 230–246.
- Zhou, J.B., Wilde, S.A., Zhao, G.C., Zhang, X.Z., Wang, H., and Zeng, W.S., 2010a. Was the easternmost segment of the Central Asian Orogenic Belt derived from Gondwana or Siberia: an intriguing dilemma? *Journal of Geodynamics*, 50: 300–317.
- Zhou, J.B., Wilde, S.A., Zhao, G.C., Zhang, X.Z., Zheng, C.Q., and Wang, H., 2010b. New SHRIMP U-Pb zircon ages from the Heilongjiang high-pressure belt: constraints on the Mesozoic evolution of NE China. *American Journal of Science*, 310: 1024–1053.
- Zhou, J.B., Wang, B., Wilde, S.A., Zhao, G.C., Cao, J.L., Zheng, C.Q., and Zeng, W.S., 2015. Geochemistry and U-Pb zircon dating of the Toudaoqiao blueschists in the Great Xing'an Range, northeast China, and tectonic implications. *Journal of Asian Earth Sciences*, 97: 197–210.
- Zhu, C.Y., Zhao, G.C., Ji, J.Q., Sun, M., Han, Y.G., Liu, Q., Eizenhöfer, P.R., Zhang, X.R., and Hou, W.Z., 2017a. Subduction between the Jiamusi and Songliao blocks: Geological, geochronological and geochemical constraints from the Heilongjiang Complex. *Lithos*, 282: 128–144.
- Zhu, C.Y., Zhao, G.C., Sun, M., Han, Y.G., Liu, Q., Eizenhöfer, P.R., Zhang, X.R., and Hou, W.Z. 2017b. Detrital zircon U-Pb and Hf isotopic data for meta-sedimentary rocks from the Heilongjiang Complex, northeastern China and tectonic implications. *Lithos*, 282: 23–32.
- Zhu, C.Y., Zhao, G.C., Sun, M., Eizenhöfer, P.R., Liu, Q., Zhang, X.R., Han, Y.G., and Hou, W.Z., 2017c. Geochronology and geochemistry of the Yilan greenschists and amphibolites in the Heilongjiang complex, northeastern China and tectonic implications. *Gondwana Research*, 43: 213–228.

About the first author



CHEN Zhaoxu, male, born in 1996; Master student of Jilin University in learning; Major in structural geology.

About the corresponding author



LIU Yongjiang, male, born in 1964; Doctor of University of Salzburg; Professor of Ocean University of China; Major Research Fields: Structural geology, Rheology and Tectonics. E-mail: liuyongjiang@ouc.edu.cn.